Instituto Superior de engenharia do Porto

Energy Harvesting for Autonomous Underwater Vehicles

Joram Van Regemortel

A thesis
submitted in partial fulfillment
of the requirements for the degree of

Master of Electrotechnical Engineering
Power Systems

Promoter: José Miguel Soares de Almeida
Co-promoter: Betina Baere De Faria Campos Neves

June 23, 2015

Acknowledgements

I would like to thank Prof. José Almeida and Prof. Betina Neves for all the help and guidance they provided me on this project. They were always available for answering the abundant questions I came up with, and they taught me a lot in the period I could be in their laboratory. Without them it would have been impossible to complete this work. I am also very grateful for being presented with this fascinating topic and involving me in the TURTLE project. I am as well very thankful to all the people in the LSA/INESCTEC laboratory for helping me when needed and for giving me a comfortable feeling when I was in the laboratory. In the same manner, I would like to thank KULeuven and ISEP for all the things they taught me in the past years.

Last but certainly not least, I want to thank my parents for motivating and encouraging me during my whole study. They were always patient and helpful with me, also during the stressful and intensive moment of writing a master thesis. Eventually I want to thank all my friends for the good moments we had together in this period, which was also necessary for finishing this work successfully.

Abstract

In this study, energy production for autonomous underwater vehicles is investigated. This project is part of a bigger project called TURTLE. The autonomous vehicles perform oceanic researches at seabed for which they are intended to be kept operational underwater for several months. In order to fulfil a long-term underwater condition, powerful batteries are combined with "micro-scale" energy production on the spot. This work tends to develop a system that generates power up to a maximum of 30 W. Latter *energy harvesting* structure consists basically of a turbine combined with a generator and low-power electronics to adjust the achieved voltage to a required battery charger voltage. Every component is examined separately hence an optimum can be defined for all, and subsequently also an overall optimum. Different design parameters as e.g. number of blades, solidity ratio and cross-section area are compared for different turbines, in order to see what is the most feasible type. Further, a generator is chosen by studying how flux distributions might be adjusted to low velocities, and how cogging torque can be excluded by adapted designs. Low-power electronics are configured in order to convert and stabilize heavily varying three-phase voltages to a constant, rectified voltage which is usable for battery storage. Clearly, different component parameters as maximum power and torque are matched here to increase the overall power generation. Furthermore an overall maximum power is set up for achieving a maximum power flow at load side. Due to among others typical low velocities of about 0.1 to 0.5 m/s, and constructing limits of the prototype, the vast range of components is restricted to only a few that could be used. Hence, a helical turbine is combined in a direct drive mode to a coreless-stator axial-flux permanent-magnet generator, from which the output voltage is adjusted subsequently by a rectifier, impedance matching unit, upconverter circuit and an overall control unit to regulate different component parameters. All these electronics are combined in a closed-loop design to involve positive feedback signals. Furthermore a theoretical configuration for the TURTLE vehicle is described in this work and a solution is proposed that might be implemented, for which several design tests are performable in a future study.

Contents

List of Figures

List of Tables

Chapter 1

Introduction

1.1 Autonomous Underwater Vehicles

In the last 10 years, underwater and seabed research and probing activities have increased the need for underwater vehicles capable of working at bigger depths and present higher autonomies. A prototype for these purposes is being developed in a project called TURTLE, in the LSA/INESCTEC lab at ISEP. This prototype of a robotic benthic lander is being constructed for civil and military stakeholders. It aims at autonomous capability of repositioning and multiple ascent and descent cycles without human intervention. Therefore, an efficient and sustainable concept of producing energy is inevitable. Both design and space limitations have imposed the search for new onboard renewable energy generation strategies. This work intends to study solutions that can help meet that goal of onboard renewable generation to be installed in this medium size underwater research and exploration vehicle, meeting ecological and design constraints.

More specifically, this report is about small-scale energy production, known as *energy harvesting*, for *autonomous underwater vehicles*. As the term "small-scale" implies, this vehicle intends to produce small ranges of power, ranging from 1 to 30 watt (W). The vehicle is launched at sea surface and further actions are controlled by technical staff onboard a ground station. Since one important goal of this project is to keep the vehicle operating underwater, for a period of several months, at depths up to 1000 meters (m), extra challenges should be considered attentively:

- Typical slow sea currents of about 0.1 to 0.5 meters per second (m/s) should be considered.
- All components should be watertight and withstand high water pressures up to 100 bar. Constructing materials and seals should therefore be chosen carefully.

- Corrosion and fouling may lead to device performance degradation.

- To assure the vehicle cannot sink away into the seabed, abundant underwater weight and high pressures must be compensated, using special foams.

- Additional logical problems associated with accessibility as e.g. maintenance or unforeseeable defects should better be prevented.

By reasons of making autonomous operation possible, adjusted communication between the ground station and the underwater robot is necessary. Control and communication of this vehicle can be ensured on the platform using an Iridium satellite and underwater acoustic modems installed in the underwater vehicle communicating with a buoy. The vehicle is furthermore equipped with several externally mounted sensors for positioning, and a velocity logger, pressure sensor, altimeter, multibeam sonar, and acoustic pinger are installed as well. Gathered data can then be observed onboard the vessel.

Since ecological awareness and lack of energy is an actual topic, several scientists have been examining renewable energy production methods for many years. Thus, existing methods can be considered for further examination leading to possible prototypes and feasible designs for energy harvesting. In this work, several energy harvesting methods, as among others, solar energy, geothermal energy and hydrokinetic energy were considered, but because of the strict requirements, only hydrokinetic energy is considered as usable. As there is almost no usable light penetrating at maximum depths of about 1000 m, solar energy would only be usable as a generation method at sea surface. Since one of the main requirements of the vehicle's operation is staying on the seabed for a longer period of time, this method is not examined in detail. Also, geothermal and wave energy are not usable here for the same reason.

Hence, one applicable topology is a turbine, driven by the passing water flow, which carries a torque to a generator by a shaft. Afterwards, this generator converts the mechanical energy to electrical, and the electrical power is in turn converted to an adequate form for storage in batteries for later use. Different low-power electronics, as a rectifier, and one or more converters ensure this regulation. A control mechanism regulates an optimal power flow between different blocks. Figure 1.1 shows an overall block diagram of a micro-power application which may be applicable in this scenario. Whether or not to implement a gear box in the design topology, can be questioned and will be discussed later on, as is marked by the different color gradient used for this block.

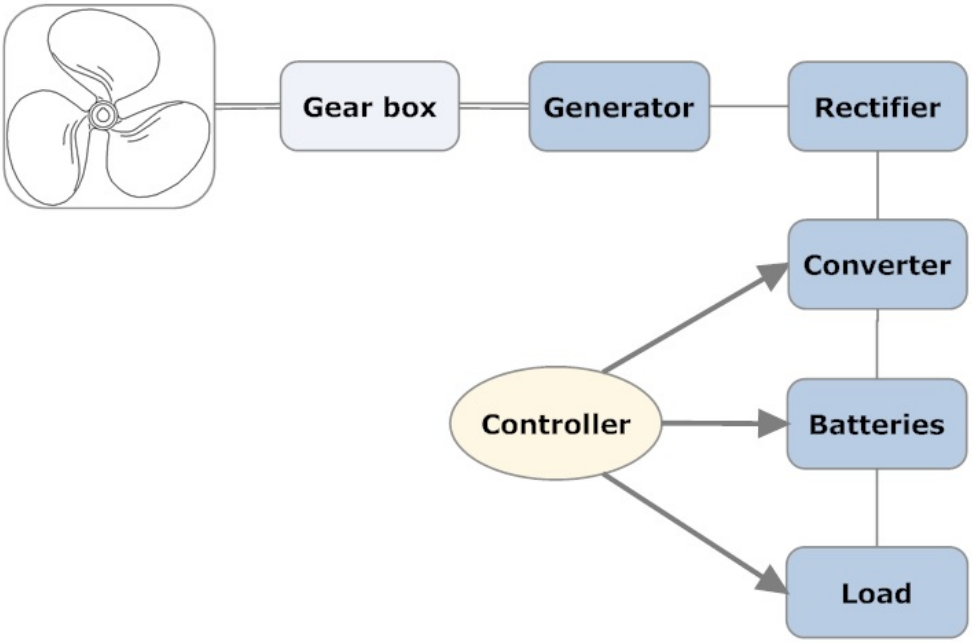

Figure 1.1: Micropower energy harvesting block diagram

1.2 Power Availability

As demonstrated by A. Khaligh and O.C. Onar [1], it is possible to calculate the maximum possible power of a delimited water flow as following:

$$P_T = \frac{1}{2}\rho A v^3 \tag{1.1}$$

Where P_t represents the available power in a certain current in W, ρ is the density of seawater, approximately around 1022 kg/m^3, A is the area of the water volume passing the turbine profile in m^3 and v is velocity of the flowing water in m/s, which is estimated between 0.1 and 0.5 m/s.

As a result of this cubed velocity factor of equation 1.1, the flow velocity might influence the output results immensely and this parameter should therefore be considered carefully, such all components must withstand both high and low ranges of electrical current. Maximum power flow is defined for each component by Joule's law, where the produced heat Q can be calculated in watt for a given current I in ampere (A), and a known electrical resistance R in ohm (Ω) over a defined time t expressed in seconds, as following:

$$Q = RI^2t \tag{1.2}$$

A minimum voltage level for normal operation of low-power electronic components as diodes, shall be defined. This minimum voltage is the minimum voltage to overcome internal voltage drops for forward biasing of the component. For instance for Silicium diodes, a typical voltage drop of 0.7 volt (V) should be taken in account. Other diode types may have other voltage drops. All these different drops decrease the remaining voltage, and hence also the output power. The amount of electronic components that are used is therefore of crucial importance. Moreover, below a specific voltage level, defined by all these voltage drops, power circuits do not operate properly any more and energy harvesting is impossible.

Efficiency should be maximized for all components such overall efficiency is at maximum for different levels of power flow. Especially for low-power productions, caused by slow-moving water flows, overall efficiency becomes more critical and should rather be optimized than the corresponding high-power levels. A general expression for efficiency can be defined as output divided by input. Thus, overall electrical power efficiency η, can be defined for an electrical output power P and a mechanical input power P_T, as following:

$$\eta = \frac{P}{P_T} \tag{1.3}$$

and P is the difference of P_T and Q:

$$P = P_T - Q \tag{1.4}$$

Nevertheless, acquiring a maximum output, still remains more important than the according efficiency. Since oceanic hydro energy is abound, and hence free, efficiency is of less importance than an overall maximized output. In contrast, e.g. coal power stations pursue maximum profits and the corresponding output efficiency should therefore rather be optimized, guaranteeing an optimal use of fuel and machinery. Thus, in case a cost is related to every produced kilowatt (kW), overall output may be less significant than the efficiency, and in case no cost is related to production, maximum output should be pursued.

Reliability of power production in this underwater vehicle, will be strongly dependent of the water flow velocity, in a way that if the water stream moves too slow, power production will be negligible, and vice versa, if the water streams too fast, and storage of the additional energy is impossible, energy shall have to be consumed by an additional dump load. A “dump load” is a resistor, which solely consumes energy in order to keep the other components within their allowed energy limits, and consequently decreases overall efficiency of the vehicle’s energy harvesting mechanism. A control mechanism, being the battery charger, regulates the power flow towards the batteries. Power must be limited by this charger to guarantee safe charging

from the batteries. These batteries are adapted such in case they are completely charged, electrical current bypasses the power cells. A different control mechanism might then regulate later power paths towards different loads. The general control mechanism is represented on figure 1.2. Batteries should be optimized for low velocities, ensuring sufficient storage capacity for providing the required energy during scarce power availabilities.

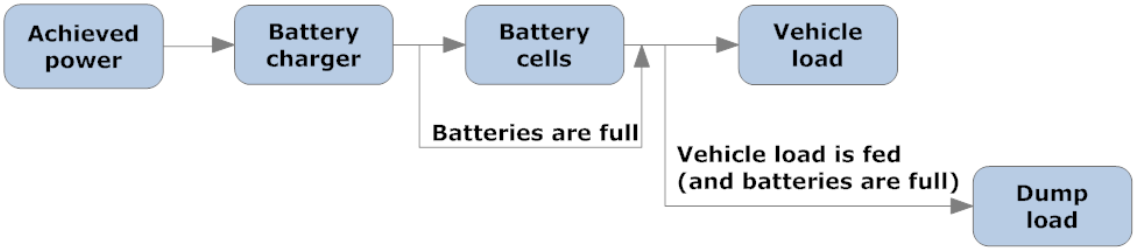

Figure 1.2: Central control mechanism of power supply.

1.3 Structure of this Work

In the first part of chapter 2 all generalities of a turbine, a generator and low-power electronics which are necessary for an underwater energy system are outlined. Further in this chapter, an alternative energy system is proposed as well. In chapter 3, the project and the energy system are described including all requirements which should be involved for this. Subsequently in chapter 4, all necessary components for developing the system are chosen and, where possible, is described where to buy or design them. Also, a proposal for a configuration is done here. Finally in chapter 5, conclusions are drawn and future work guide lines are described.

Chapter 2

State of the Art

2.1 Turbine

2.1.1 Introduction

The turbine captures a linear force of the sea current and converts this into mechanical power as rotational torque. Because velocities are, as mentioned before, deemed to be between 0.1 and 0.5 m/s at depths of 1000 m below sea level, an adapted model should be considered. Most of the preceding small-scale turbine examinations were restricted by reasons of money or time, therefore, it is very hard to find an unequivocal and existing turbine model. Macro-scale turbines are in general more lucrative and more commonly used. Hence, the majority of the researches were done for these turbines, having velocities greater than 1 m/s and having bigger dimensions. Additionally, it is hard to find an existing model, designed for our restricted requirements, one that can be bought as a unit to implement in our design. Characteristics of already existing turbines moreover have to be compared attentively, such the most suitable turbine type can be selected.

Performance Parameters

Several performance parameters are used frequently. One of them is the tip speed ratio (λ), defined as the ratio of the tangential speed of the tip of the blade to the freestream velocity (v_0). This latter is the velocity of the fluid before the body has a chance to influence this stream. If R is the radius in meters, and ω is the angular speed of the turbine in radians per second (rps), λ might be represented as [2]:

$$\lambda = \frac{R\omega}{v_0} \tag{2.1}$$

Another parameter is the power performance coefficient (C_P), represented as the ratio of the shaft power output (P_S) to the obtained mechanical power input [2]:

$$C_P = \frac{P_M}{P_S} \tag{2.2}$$

A maximum power performance coefficient of $\frac{16}{27}$ is theoretically defined by Betz and is proven in previous studies [1].

Venturi Effect

Since the majority of the turbines make use of the *Venuri effect*, it demands a basic explanation. Adapted blade airfoils can induce additional rotational torque on the blades, and the Venturi effect is the main reason of this induction.

As known by this law, velocities of the fluid (v_1 and v_2) and pressures of the fluid on the resulting surface (p_1 and p_2) are proportionally correlated. This is described by the following formula, where ρ represents the density of the fluid:

$$p_1 - p_2 = \frac{\rho}{2}\left(v_2^2 - v_1^2\right) \tag{2.3}$$

An example of the resulting lift force on an airplane wing, induced by the Venturi effect, can be observed on figure 2.1.

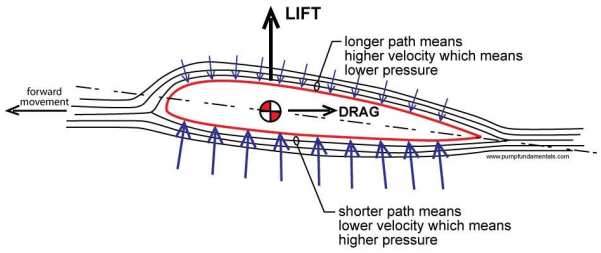

Figure 2.1: Resulting lift force on air plane wing induced by Venturi effect [3].

2.1.2 Drag and Lift Types

There are two different types of turbines [2]. A first group consists of drag type devices. Here, forces are principally induced by the pressure of pushing water on the blades or cups of the rotating rotor. The shape of the cups is adapted such that forward moving cups encounter bigger forces than backward moving cups. The Savonius turbine is the most common example

of a drag style turbine and is illustrated for a wind turbine on figure 2.2, which has, in fact, the same operating principle as for a hydro turbine.

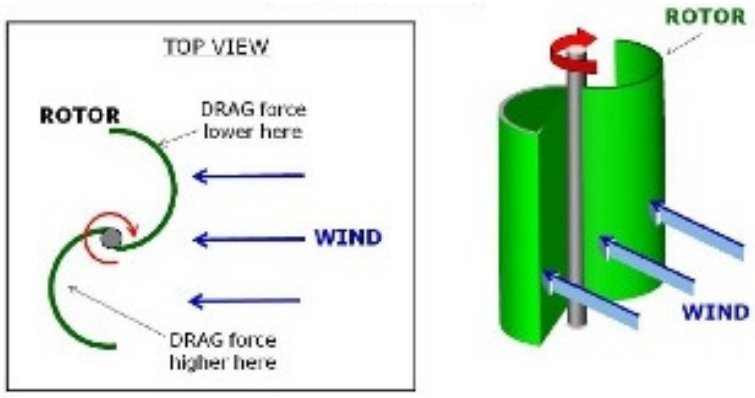

Figure 2.2: Forces on forward and contrary moving cups of a Savonius drag style turbine [4].

A lift type device is the other common turbine type. In contrast to drag types, this group mainly uses lift forces. A resulting lift force is induced by the fluid flowing around the airfoil profile. This force is directly proportional to the angle between the incoming fluid flow and the airfoil chord line, better known as the angle of attack (α). The Venturi effect causes a difference of pressure on both sides of the blades, resulting in an upward force. The lift force acts here perpendicularly to the relative fluid velocity. A drag force additionally occurs, because of the moving blade surface against the incoming fluid. Logically, this is disadvantageous for the overall torque production. Both velocities and force vectors can be observed in figure 2.3. F_L is the lift force, F_D is the drag force, F_T is the tangential force, F_N is the normal force, u_s is the stream-wise velocity component on the blades (which is a part of the freestream velocity), ωR is the rotational velocity of the rotor and u_{REL} is the relative velocity component of the rotor [2].

Compared to lift types, consisting out of complex designs, drag style devices are in general easier to design because they are made of simple bowls. Drag devices mainly have lower angular velocities than lift types which makes them less efficient too. Thus, efficiency is better for lift style devices because tip speed may here be faster than the resulting water stream velocity, which is impossible for drag devices [2].

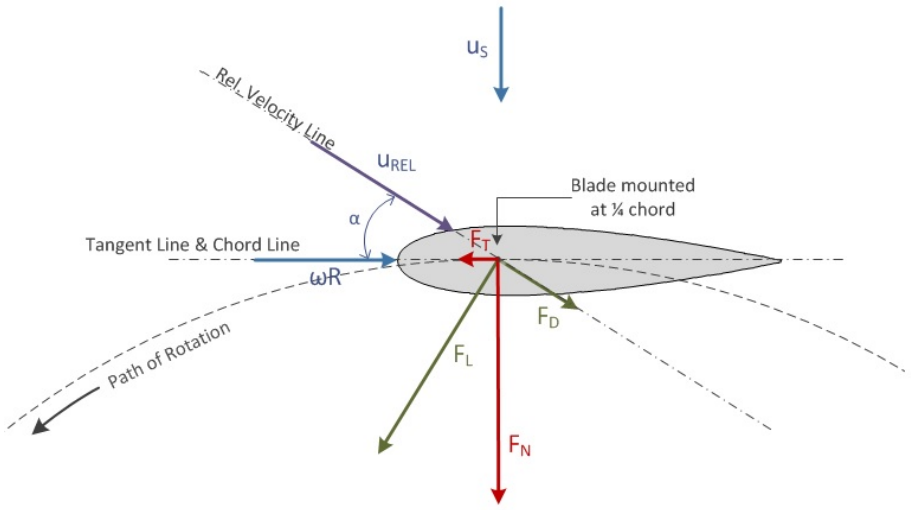

Figure 2.3: Velocity and resulting lift force vectors for an airfoil [2].

2.1.3 Axial and Cross-Flow Turbines

Turbines can also be classified according to their orientation to the resulting stream flow. Axial-flow and cross-flow turbines can be differentiated here as illustrated on figure 2.4. Axial types have their turbine profile oriented towards, or 180 degrees against the incoming current stream, which makes them more efficient. Consequently, a disadvantage is the need for a parallel alignment according to the incoming fluid stream. For cross-flow turbines, the incoming direction of the stream does not influence power production, which might be profitable for difficult accessible underwater turbines. Unfortunately, efficiency also decreases for this easier design [2].

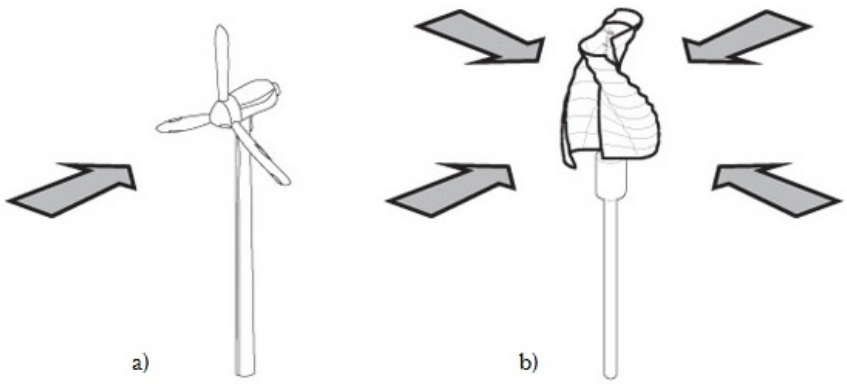

Figure 2.4: a) Axial-flow turbine b) cross-flow turbine [5].

2.1.4 Types

Three-Bladed Windmill Design

A first creation of an axial-flow turbine has a typical windmill design of three blades. The amount of blades may be different, but three-bladed turbines are most commonly used in micro-scale projects, like underwater vehicles. An appropriate orientation of the rotor is of great importance for this case. Macro-energy production as tidal energy projects make often use of three-bladed turbines, because tidal water currents can be calculated accurately, where orientation of the turbine can be adjusted adequately according to the alternating current direction, so that gained power can be maximized easily.

Naturally, this type is also used in micro-scale power, e.g. on boats or yachts where additional battery charging current is required. An example is shown on figure 2.5 [6]. The Ampair Aquair Underwater 100 has a rotor of 312 mm with an integrated generator of 24 W in a 2 m/s water current. Hence, in this case the turbine must be pointed to an appropriate direction.

Figure 2.5: Aquair UW [6].

An example of a macro-scale three-bladed turbine is shown on figure 2.6 [7]. For this tidal energy example each blade is 1.6 m long and sea currents were expected to be between 1 to 3 m/s. In figure 2.7 characteristics for power, torque and thrust to the appropriate flow-speed of this developed macro type are shown. This turbine is less profitable for low velocities, but still remains a valid solution.

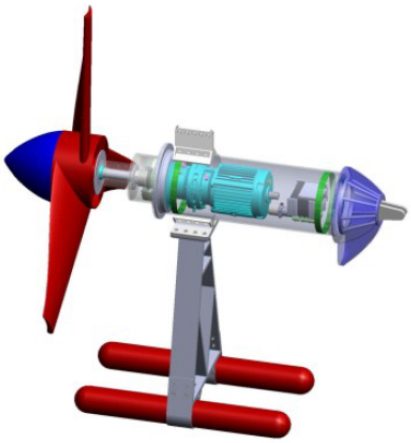

Figure 2.6: Macro-scale three-bladed axial-flow turbine [7].

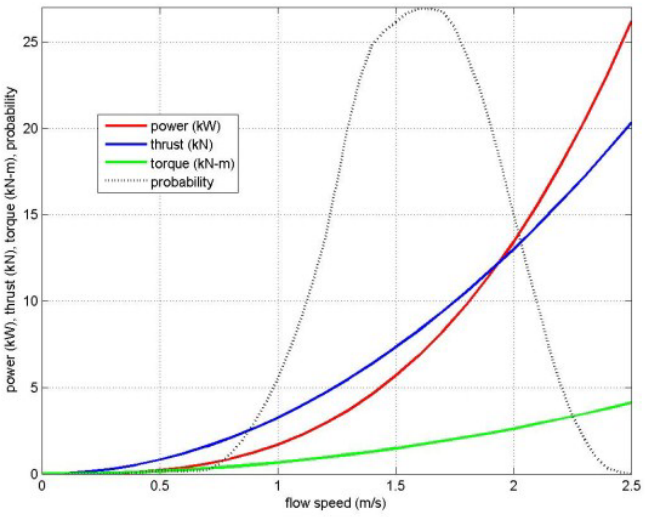

Figure 2.7: Maximum power, torque, and thrust predicted for different water-flow speeds for a three-bladed axial-flow rotor [7].

Shrouded Three-Bladed Design

An improvement of the prior three-bladed windmill-type turbine, is a shrouded-type [8]. In this model, a shroud surrounds the turbine inducing larger amounts of fluid passing the blades to increase the torque on the blades, as is shown in figure 2.8. The earlier mentioned Betz limit of $\frac{16}{27}$ logically still holds. To calculate the power performance coefficient correctly, the outer area of the shroud must be considered.

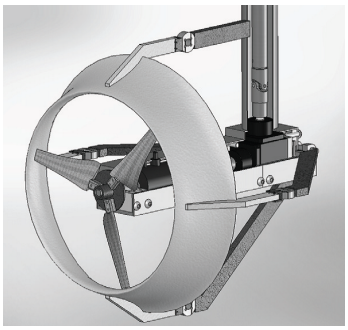

Figure 2.8: Shrouded turbine [8].

Savonius Rotor

A Savonius rotor is a typical example of a drag style device, which can be aligned having a horizontal or vertical axis. Such a design is easy and cheap to manufacture. Generated rotor shaft torque is high and tip speed is low. Consequently, tip speed ratio will also be low and so does efficiency. This design is therefore disadvantageous, because low tip speed ratio can make break-away torque too high, where rotor cannot start turning any more. Figure 2.9 illustrates an example of a Savonius rotor [2].

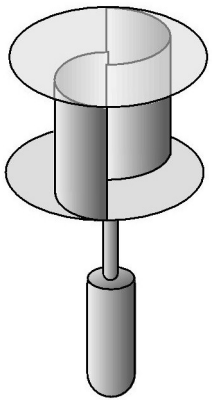

Figure 2.9: Savonius rotor [9].

Darrieus Turbine

The Darrieus turbine is another type which is mostly vertically aligned [10, 11]. This model is a typical example of a lift type device. On the following image of figure 2.10 an example of the Darrieus turbine is shown.

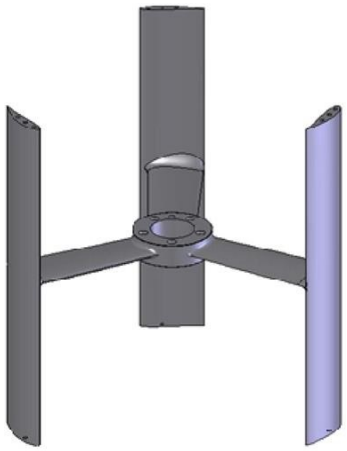

Figure 2.10: Darrieus turbine [11].

An advantage of this turbine type is the high tip speed ratio, increasing the rotational speed as well. Since most generators require high rotational speeds for efficient energy production, an appropriate match for these speeds causes better overall power results. Tip speed can for this type be even bigger than the surrounding water flow. On the other hand, lift force is submissive to flow velocity, and is therefore still a decisive parameter for the overall produced torque. Moreover, due to the discrete blade angles, and the low starting torque, self-starting can still be a common problem for low water-flow speeds. Turbines with a higher number of blades are subject to a more constant torque and therefore to less undesirable influence. Results show that the rotational angle of the rotor does not affect the resulted torque very much. The angle of attack alters for different relative positions, and this angle is proportional to the gained torque. Hence, if the blade number is higher, torque remains more constant for alternating rotational angles. Although, a frequent problem for these right-aligned blades, is an inherent torque oscillation for low tip speed ratios [2].

A schematic of a three-bladed Darrieus turbine is shown in figure 2.11. For this turbine, U_∞ represents the freestream velocity, W is the stream-wise velocity, V is the tangential blade velocity, and α the angle of attack. D and L are the induced lift and drag forces. It reads that the drag is always parallel to the attack velocity modulus W, and the lift perpendicular to this velocity [11].

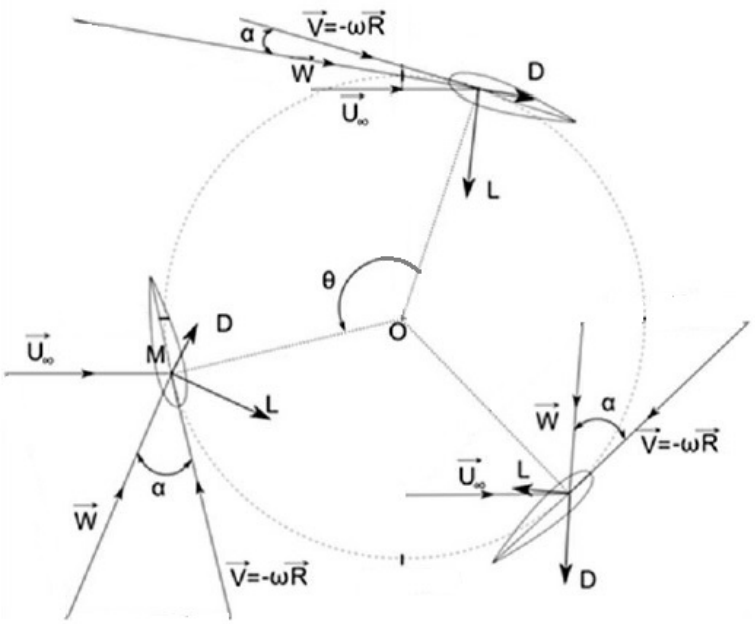

Figure 2.11: Resulting forces of drag and lift on Darrieus turbine blades [10].

Both forces can be calculated approximately using complex models [2]. Since the attack velocity is hard to define for each blade separately, it might be more adequate to run a simulation.

Moreover, calculated results can be influenced by the rotating blades' induced vortices. Figure 2.12 shows a simulation of how these vortices might look like for the three-bladed turbine of figure 2.10 [11]. This figure represents the complexity of water streams making calculations hard as well.

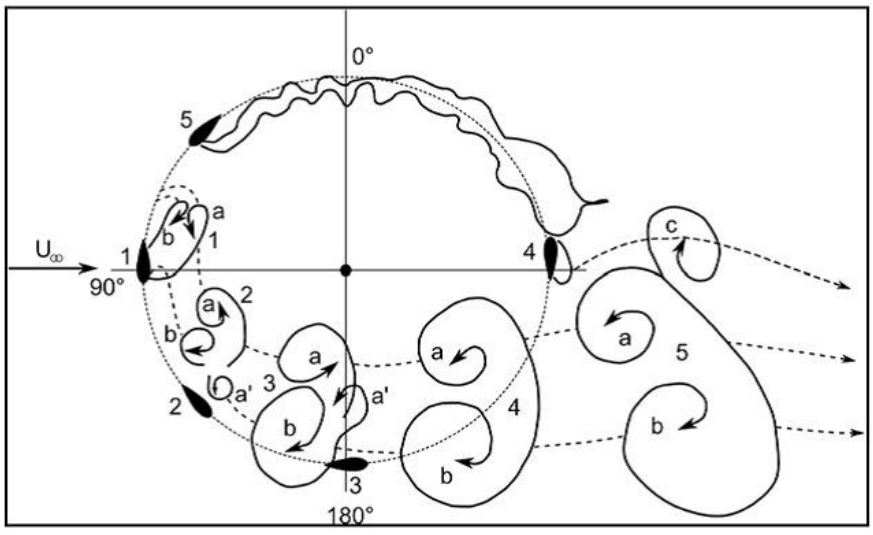

Figure 2.12: Simulation of vortices that are induced by a Darrieus turbine [11].

Hybrid Turbine

For both the self-start problem and the alternating torque from the Darrieus turbine, the hybrid turbine leads to an improvement. A Darrieus turbine and a small Savonius rotor are connected on the same rotational axis in an attempt to diminish these phenomena. This solution can be beneficial for the self-start, but complexity to find an optimum for both turbines increases as well. While a Savonius rotor operates optimally for tip speed ratios lower than 1, a Darrieus turbines' optimum can be found much higher than 1 [2]. One example of a wind hybrid type consisting of two twisted Darrieus blades, and two perpendicularly placed Savonius rotors in between, is shown on figure 2.13.

Figure 2.13: Hybrid turbine [12].

Helical or Gorlov Turbine

A helical or Gorlov turbine is similar to a Darrieus straight-bladed turbine, except for the fact that the blades are swept here in a helix profile. Figure 2.14 presents an example of a helical turbine.

Compared to the straight-bladed Darrieus type, one advantage of this type is the more fluent self-start. Due to the helical shape sweeping along the circumference, some portion of the blade profile will always be located at the optimum angle of attack. Consequently, dependency of each blade position reduces, which is beneficial for both self-start and torque oscillation. Logically, all different angular positions of the circumference should be covered by at least one helical blade. The circumference can be covered by more blades as well, but all angular positions should in any case see the same amount of blades to minimize torque alternations. The percent that the blades span collectively along the radial circumference is expressed by the *blade wrap*, and is

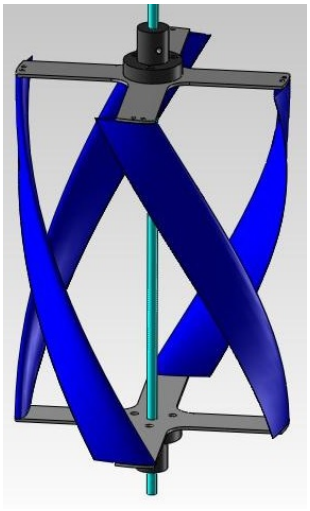

Figure 2.14: Helical turbine [2].

thus best 100%. Additionally, self-start improves for a lower blade number and power results are influenced oppositely.

2.1.5 Blades

Many profile shapes can be considered, for which several parameters have to be set up first. An airfoil profile is dependent on these parameters, and power results are therefore heavily influenced by this choice. Pressure and force differ according to among others, the chord length, leading edge profile, trailing edge profile, blade thickness-to-chord ratio, location of maximum thickness and blade camber. Furthermore, a wide range of angles of attack with consequently low drag, high lift-to-drag ratio and high maximum lift coefficient were preferred for optimal performance. An extensive analysis found which type of blades meet these requirements the best[2]:

- Cambered blade, with camber facing concave outward, away from the radial direction;
- Thick blade profile;
- Large leading edge;
- Sharp trailing edge;

The optimum lift was subsequently found for negative angles of attack and for symmetric airfoils. Negative angle of attack means in this case an angle towards the convex, outer side of a cambered airfoil, as is clearly illustrated in figure 2.15.

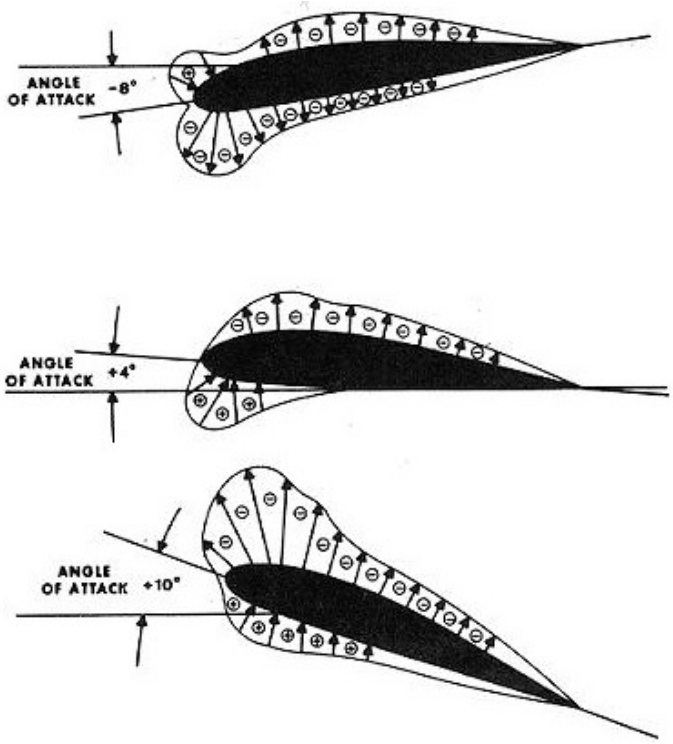

Figure 2.15: Positive and negative angle of attack [13].

Self-starting is an important aspect that must be considered attentively for low velocities. One way to modify this characteristic is to change the amount of "solidness" of a turbine. In an attempt to represent this parameter, a solidity ratio is defined. In literature many different definitions show up, but for this present study it will be declared as following:

$$\sigma = \frac{Bc}{\pi D} \tag{2.4}$$

Here represents B the number of blades, c the chord length and D the turbine diameter. A high solidity ratio (σ>0.3) implies an easier self-start, but decreases the tip speed ratio. A low solidity ratio (σ<0.15) does the opposite [2].

The number of blades seems to be directly proportional to the solidity ratio. For a higher number of blades, the chord length must be reduced in order to keep an optimal solid ratio. The number of blades will also influence the power coefficient for airfoil shaped blades. As the amount of blades increases, the corresponding power decreases, and so does the power coefficient. Hence, generated power is influenced by both solidity ratio and number of blades. Unfortunately, self-start is influenced in the opposite way, for what a compromise between the two always should be considered [2].

Another parameter is the aspect ratio AR, which is defined as:

$$AR = \frac{L}{c} \tag{2.5}$$

where L is the spanwise blade length, and c the chord length. Analyses proved that the coefficient of performance improved for aspect ratios up to 12:1, but starting torque coefficient was inversely proportional to the aspect ratio [2].

The cross-section area, represented here as A, is the product of the height H, and the diameter D:

$$A = HD \tag{2.6}$$

This is shown in figure 2.16. For a larger cross-section area, longer blade length is required. Consequently, for increasing length, midspan blade support must be considered for reducing mechanical phenomena as deflection, vibration and stress on the blades [2].

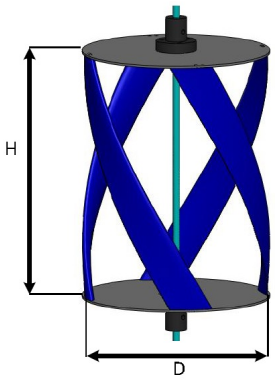

Figure 2.16: Height and diameter to represent cross-section area for a helical turbine [2].

The helical pitch angle, δ is for a vertical axis turbine the angle between the blades and the horizontal plane as is explained on figure 2.17. Greater pitch angles result in better power coefficients, but will also increase starting torque and cause higher torque alternations. These mechanical fluctuations will appear as harmonic content in the electrical values produced by the generator. For better overall results it is therefore better to avoid this fluctuation. Hence, this is another way of explaining why self-starting is such a problem for Darrieus turbines. Again a compromise must be considered.

In addition, other parameters as e.g. angles for blade rotation according to their own transverse axis can be examined, but are not studied here.

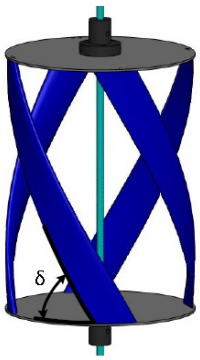

Figure 2.17: Pitch angle for a helical turbine [2].

2.1.6 Vortex Generator

Big aircraft wings often contain a row of small shaped vortex generators, attached on top of the airfoil for inducing extra lift force. In fact, these vortex generators act like miniature wings, creating additional lift forces perpendicular to their own surface. As can be seen on figure 2.18, these features have a typical design. They can be installed at airfoil blades in one long horizontal row as shown on figure 2.19.

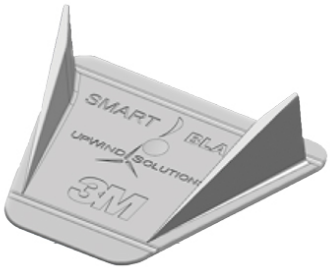

Figure 2.18: Vortex generator [14].

Big windmill airfoil blades are very difficult and expensive to design. A problem that occurs for classic windmill blades is the airflow separation, known as *aerodynamic stall*. Here, efficiency consequently reduces. Windmill blades have a twisted stall design to obtain more wind force. Optimizing this shape, such this wind separation does not appear too much. Therefore, vortex generators are applied for big blades for several years now. Increasing blade efficiencies is much easier by adding these features than by optimizing the shape of the airfoil, requiring complex mathematical models [16].

Figure 2.19: Airfoil blade with attached vortex generators [15].

Because of the vortex generator, vortices are induced to create extra lift such the boundary air layer retains attached at the airfoil. As is illustrated for airplane wings on figure 2.20, the vortex enables bigger angles of attacks, and thus bigger torques are induced as well. This principle is exactly the same for airplane wings as for windmills. The term "vortex generators" is on this figure abbreviated as "VGs".

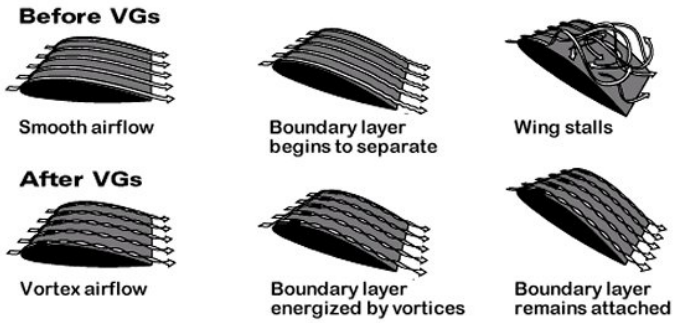

Figure 2.20: Effect of Vortex generators on boundary layer [17].

As is represented on figure 2.21, this boundary air-layer height decreases because of the interaction with vortex generators. Also, the separation of this air layer decreases because of this. The shape of the vortex generator is designed in a way that airflow is redirected. Separation of air layers can be minimized by counteracting adverse interactions between similar airflows. A result of this is a more smooth flow which is also closer to the airfoil, and encounters additionally a higher energy density [16].

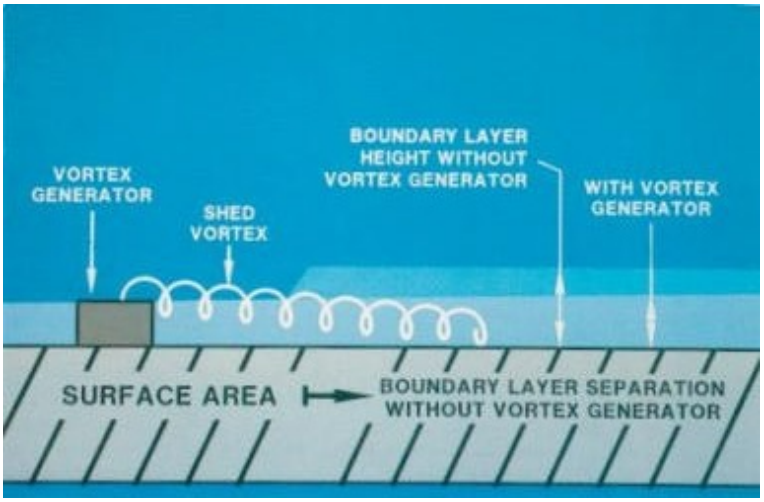

Figure 2.21: Reducing effect of VG on the boundary layer height and on the boundary layer separation [16].

So far, this technique is only applied in wind applications as e.g. wind turbines and airplanes. It has not been used for hydro turbines until now, but here it may be an improvement as well. Results for windmills were mostly obtained experimentally, and since water flows can differ from air flows, many tests will be necessary. Additionally, the slow velocity and the high pressure of the fluid stream shall have to be taken in account as well. In any case, this adaptation may be a substantial addition to an existing turbine and it is definitely worth further examination in a future work.

2.2 Generator

2.2.1 Introduction

Basically, a hydrokinetic force of an oceanic water stream is converted into a rotational torque by the turbine, and will in turn be delivered by a shaft to the rotor of the generator. The generator tends here to convert kinetic power to electric power. Logically, no connection to a feeding grid is possible for an underwater vehicle which aims to operate at high depths. The generator must therefore be a stand-alone unit, and generator excitation should be adapted to this.

Another thing is to compare different component characteristics to each other, pursuing an overall optimum. Ideally, the optimum of the generator is matched to both turbine and low-power electronics optimum. The preferred solution would mean developing a matching generator at the lab, since commercially available solutions will only approximate our intentions and are somewhat scarce in numbers. This scarcity is imposed by the conditions and values to deal with, like water velocity, weight, shape, just to mention a few. Unfortunately, the 3 month period assigned to this work made it impossible to consider the very desirable approach of building everything at the LSA laboratory.

2.2.2 Generator Types

Mainly, there are three categories of generators: induction or asynchronous, synchronous and DC generators. Seeing that our examined sea flows are very slow, a choice for a suitable generator must be considered attentively.

Asynchronous or Induction Generators

Asynchronous or induction generators are in fact motors, but they are driven by an external source. These generators produce power directly proportional to the difference in speed of a point on the rotor to an induced magnetic rotating field. This phenomenon of speed difference is typical for induction machines, and is called *slip*. Opposite pole pairs on the stator induce a rotating field seen by the rotor. Slip between the rotor and this magnetic field is necessary to carry power from the stator to the rotor or vice versa, dependent whether a motor respectively a generator is considered. As a result of this general principle, the rotor should turn faster than this rotating field to generate power, which is impossible for low velocity conditions. Furthermore, little power alternations provoke big speed variations, for what this type is rarely used in stand-alone modus.

Synchronous Generators

Synchronous generators are in contrast to asynchronous generators not dependent on this slip phenomenon. However, synchronous generators with excitation provided by permanent magnets still require high speeds, much too high for what we need. They usually are not meant to work with highly variable speeds too. Thus, they differ from the permanent-magnet (PM) generators we are considering for this work. PM generators will be used, but they will be adapted in a way that a highly variable output is still usable. Their design is modified to reduce leakage fluxes so that power may be generated at low velocities.

DC Generators

A DC generator needs electromagnets or permanent magnets as excitation providers [18]. Output voltage and frequency can here be regulated easily by modifying the excitation flux. One decisive drawback which makes this generator type unusable, is the necessity of a commutator and brushes. Since rotating generators always produce an alternating voltage, brushes and an a commutator are used for commutating the voltage mechanically. Consequently, disadvantageous friction is induced, which might reduce efficiency heavily at low angular velocities. Additionally, maintenance of such an item is often required. This is not compatible with the autonomy and reliability meant for the underwater vehicle.

2.2.3 Cogging Torque

The *cogging torque* is a phenomenon caused by the interaction of permanent magnets of the rotor and iron cores of windings of the stator, implying magnetic alignment or attraction for which an effect of "braking" or opposing the rotational movement occurs. This effect, shown on figure 2.22, can in its most fundamental form be expressed as [19]:

$$T_{cog} = -\frac{1}{2}\Phi_{\delta}^{2}\frac{dR_{\delta}}{d\theta} \tag{2.7}$$

where Φ_{δ} is the air gap flux expressed in weber (Wb), R_{δ} is the air gap reluctance in ampere-turns per weber ($\frac{nI}{Wb}$) or in turns per henry ($\frac{n}{H}$) with a number of turns n, and θ is the mechanical angular position of the rotor in radians. For this most fundamental equation, magnetic saturation and other ending effects, as e.g. finite width of poles are neglected.

This cogging torque process encounters a cycloidal changing movement [19]. The period might be adapted here changing the proportion of pole (or tooth) numbers and slot numbers.

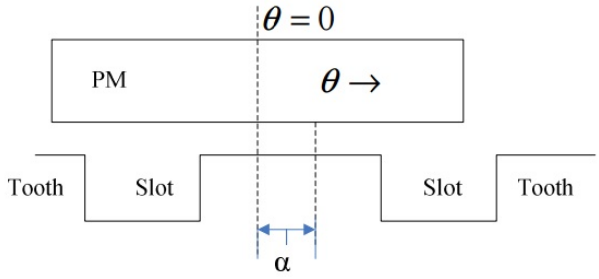

Figure 2.22: Scheme of occurring cogging torque [19].

In general, for less slots or poles, and for larger mathematical common multiples between the slot number Q and the pole number $2p$, the lower the amplitude of the cogging torque will be.

Furthermore, also the length and shape of the magnet pole arcs can influence the cogging torque. Since different pole arcs lead to different flux density distributions in magnets and air gaps, cogging torque might alter according to the modifying flux field. It reads, an optimal pole arc length can be found experimentally by changing the pole length. This is expressed by a ratio α_p, representing the pole length compared to the periodic length of a pole and a slot.

Additionally, both of these influences can be simulated using Fourier analysis, and an optimum can be found based on finite element analysis as well [20].

2.2.4 Gear Box

According to G. Madescou et al. [21], a gear box should be avoided here because of its inherent losses. Nevertheless, for obtaining good power results, slow speeds should be compensated in another way. By adding e.g. appropriate power electronics the output voltage of the generator can be upconverted which is necessary for achieving higher efficiencies. An adequate generator shall furthermore be selected in accordance to low speeds. Recently, lots of adapted generator types are optimized for slow angular velocities and are becoming available commercially.

In most macro-scale power plants, as big hydropower plants or wind farms, shaft speeds might easily be matched using a gear box. An optimal generator and its optimal rotational speed can thus be found for those cases. Gear box losses seem to be substantially lower than overall losses that the plant encounters. Furthermore, losses are not that decisive because the obtained wind or hydro energy is free. It might thus be cheaper for building a power plant using a gear box and a commonly used high-speed generator instead of expensive generators especially adapted at low speeds.

For small-scale energy harvesting in contrary, this particular loss is much more decisive. The high-depth power scarcity requires an optimal power harvesting approach, for which all losses should be reduced the most as possible. Hence, seeing our specific conditions it might here still be considered using a more expensive low-speed generator, instead of a cheaper high-speed equivalent from which the speed is decreased by a gear box. Reasons of money are moreover considered to be of secondary importance in this case.

The generator output voltage E_f is directly proportional to the angular velocity, and as the angular velocity is low, the output voltage will be low as well. If k is an inherent machine constant, N the angular velocity in revolutions per minute (rpm), and Φ the magnetic flux in weber, this output voltage or *electromagnetic force* (EMF) is expressed by equation 2.8, proving easily the directly proportional relationship between speed and EMF:

$$E_f = kN\Phi \tag{2.8}$$

Additionally, the machine constant for generators can be defined:

$$k = \frac{Np}{2\pi a} \tag{2.9}$$

where $2p$ represents a pole pair and thus p one pole, and a the number of wounded coils for EMF induction. Seeing equation 2.9, the used pole pairs are directly proportional to the output voltage.

A considerable generator for which a gear box is unnecessary contains therefore more pole pairs to compensate the low rpm. It yields that output voltage increases for more pole pairs and this is necessary for efficient power production.

2.2.5 Magnets

Many types of wind and hydro generators can be considered, but the majority of them are synchronous generators using magnetized coil cores which are excited by an external DC current. Yet, this technique is not usable for low-power production because electrical losses for inducing magnetic fluxes in the coils, are no longer negligible for such low powers. Therefore, *permanent magnets* (PM) are inevitable because they are not supposed to deal with any electrical loss at all.

When an external magnetic field is applied across a ferromagnetic material, as e.g. iron, atomic dipoles may orientate themselves according to this external field. When this field is then removed later, the altered orientation of the dipoles will retain partly, resulting in magnets that provide an own magnetic field. The effect of remaining magnetization is the so-called *remanence*. Disadvantageously, designed magnets may demagnetize by applying a strong reverse magnetic field, heavy shocks, heat, or by reasons of time. PM's pursue to avoid this demagnetizing process, to retain sufficient energy for inducing a voltage across the stator coils. Therefore, hard magnets are commonly used for permanent magnets, meaning that their dipoles do not easily alter alignment, and consequently demagnetization is limited. Iron provides good magnetic characteristics and is an often used material in e.g. transformators or generators to create a magnetic circuit. Rare-earth sintered magnets such as neodymium-iron-boron (NdFeB) are e.g. one feasible type of permanent magnets meeting hard magnetic characteristics [21, 20].

2.2.6 Radial and Axial Flux

Magnets of a PM generator are mostly configured radially to the rotor. In general, results are good for this topology because an easy mechanical structure of the rotor can be used which inherently reduces losses. On the other hand, radially mounted magnets might overcome many drawbacks of axially-mounted magnets, as e.g. better power generation at low speeds. Both structures are as a first illustration compared on figure 2.23.

As explained in [20, 22], *axial-flux* permanent-magnet (AFPM) machines generally have a more compact diameter to flux ratio compared to radial flux machines, leading to compacter designs. Higher pole numbers are therefore easier to implement, and according to equation 2.8 higher stator voltages will be induced. Hence, for low-speed applications axial-flux generators are preferable because higher pole numbers might compensate the slow speeds.

Additionally, cogging torque can decrease when an adapted topology of axial magnets is used, and undesirable magnet core attractions can be excluded. In a traditional radial configuration, the stator contains radially oriented windings which might be eliminated in axial coreless-stator machines.

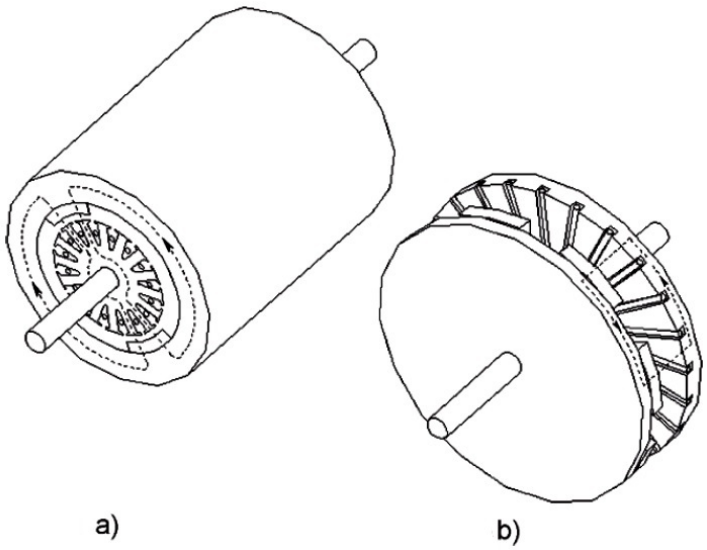

Figure 2.23: a) Radial-flux generator, b) axial-flux generator [20]

2.2.7 Coreless-Stator AFPM Machine

Design and Generalities

The cogging torque can be reduced by creating *coreless-stator* structures that eliminate permanent magnets on the rotor, and thus exclude magnetic interaction to the stator windings. According to Gieras et al. [20], any ferromagnetic material should be eliminated in the cores. The radial permanent magnets of the rotor are here changed by their axial equivalents. Single, double, triple, and eventually more rotors, are subsequently combined with composite or non-magnetic stator(s).

On figure 2.24 a twin-rotor coreless type is represented. Permanent magnets are placed on the rotors, such a smooth side surface is realized on top of the magnets. In this way, eddy currents and hysteresis losses are eliminated. Flux densities stabilize and improve here as well. Consequently, cogging torque is excluded, which is the desired effect of this design. Output torque will increase and the shocking effect of the alignment of magnets disappears. Also, the overall inertia of the system reduces, and thus no extra start-up energy is required. On the other hand, this structure requires more PM material for compensation of the decreased magnetic flux, for which a higher material cost emerges. Composite or fiber-glass non-magnetic materials are used to hold the coreless windings of the stator together. There are also other solutions, but a non-magnetic metal should be considered in any case, because the characteristics of the chosen material can influence the flux distribution and correspondingly the cogging torque. For the rotor poles, rare-earth magnets with axial magnetization are used [20].

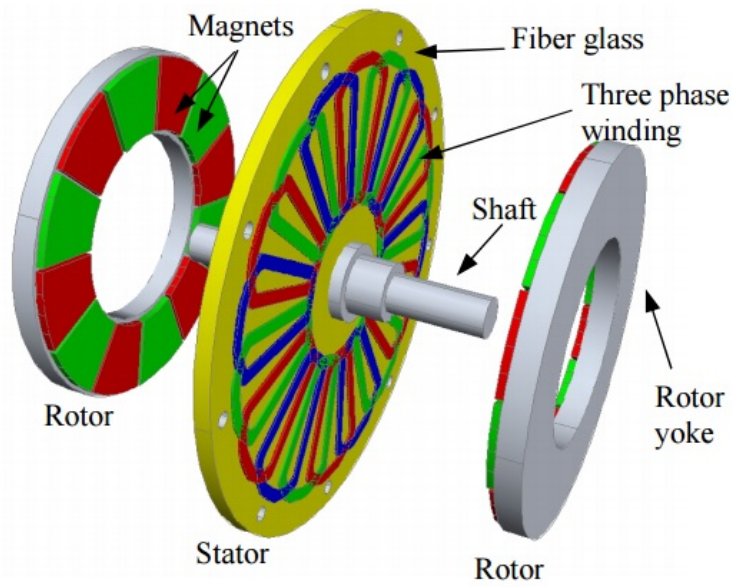

Figure 2.24: AFPM twin-rotor coreless-stator generator [22].

Magnetic and Electrical Equivalent Circuit

A non-negligible amount of leakage flux must be considered, because losses occur between mutual magnets of the same rotor, represented by Φ_{mm}, and also between the proper magnets and the rotor yoke, Φ_{mr}. These losses must be minimized by choosing an adequate magnet geometry and minimal airgap distance. Both losses are shown schematically on figure 2.25 and are calculated experimentally in [22].

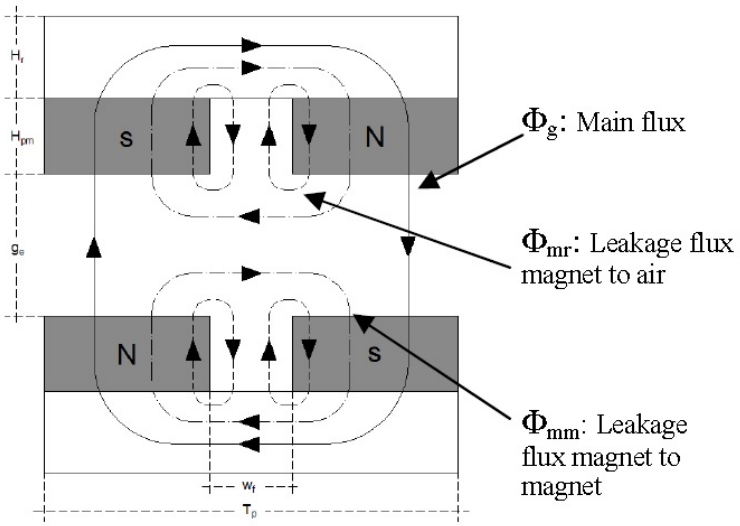

Figure 2.25: Axial-flux composition, showing different losses [22].

In order to compose a magnetic and electrical equivalent circuit, some parameters shall be declared first. Since an inevitable amount of flux leaks away, as consequence of mutual coupling of magnets, and magnet to rotor yoke losses, two new flux parameters can be introduced: X_a is the armature reactance for what mutual magnet flux Φ_{mm} and magnet to rotor yoke flux Φ_{mr} are the magnetic source and the magnetizing characteristic of the iron armature structure enlarges this loss, and X_1 is the stator leakage reactance, which is induced by the magnetic field of the stator current and opposes the main magnetic flux field. Additionally, the synchronous reactance can be declared as the sum of the armature reaction reactance X_a and the stator leakage reactance X_1:

$$X_s = X_a + X_1 \tag{2.10}$$

Further, considering an orthogonal dq-coordinate system, for which the d-axis is set horizontally and the q-axis vertically, X_a can be split up as following:

$$X_a = X_{ad} + X_{aq} \tag{2.11}$$

More, R_1 is an electrical stator resistance, R_e is a shunt resistor which is electrically proportional to the stator eddy current losses, E_f is the EMF induced in the stator winding by the rotor PM excitation system, E_i is the rms value of the internal phase voltage (including opposing armature losses), and V_1 is the terminal voltage (including electrical and stator leakage losses). The rms stator current I_a is the load current induced in the stator. Latter parameter can consequently be split up according to a dq-coordinate system:

$$I_a = I_{ad} + I_{aq} \tag{2.12}$$

Hence, eventually on figure 2.26 an electric steady-state equivalent scheme of an AFPM machine may be observed. Equations can be found for load impedance Z_L. A scheme of this circuit is shown on figure 2.27. Z_L is the sum of load resistance R_L, and load reactance X_L which consists of an induction L_L and a capacitance C_L:

$$Z_L = R_L + j\omega L_L - j\frac{1}{\omega C_L} \tag{2.13}$$

The stator current I_a can be calculated by Ohm's law:

$$I_a = \frac{E_f}{\frac{R_e\sqrt{(R_1+R_L)^2+\left(\omega L_s+\omega L_L-\frac{1}{\omega C}\right)^2}}{R_e+\sqrt{(R_1+R_L)^2+\left(\omega L_s+\omega L_L-\frac{1}{\omega C}\right)^2}}} \tag{2.14}$$

Other circuit parameters can be calculated analogous using basic resolving methods for electric circuits.

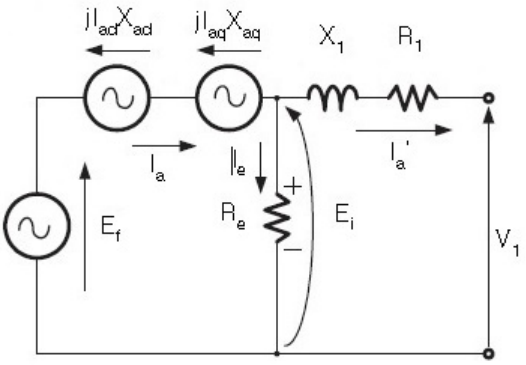

Figure 2.26: Electric scheme of AFPM machine [20].

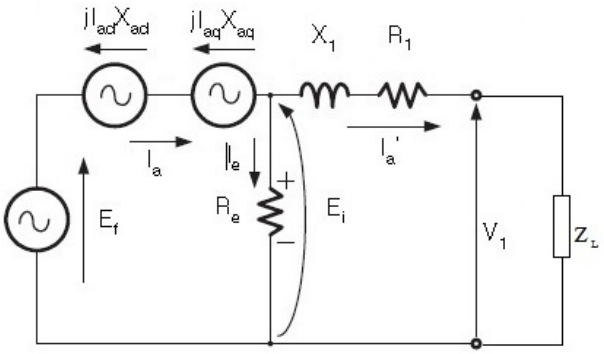

Figure 2.27: Electric scheme of AFPM machine with a connected load [20].

Characteristics

On figure 2.28, representing a comparison of the induced EMF per phase E_f and phase voltage V_1 versus speed n, load current I_a versus speed n, output power P_{out} and input power P_{in} versus speed n and efficiency η and power factor $pf = \cos\phi$ versus speed n. On these graphics, E_f, V_1 and I_a seem approximately linear proportional to the angular velocity. Power production increases more than linearly proportional. Power factor decreases for higher angular velocities, because magnetic losses increase for higher values, caused by saturation reasons. Efficiency remains better for a bigger interval of angular velocities because cogging torque can be eliminated.

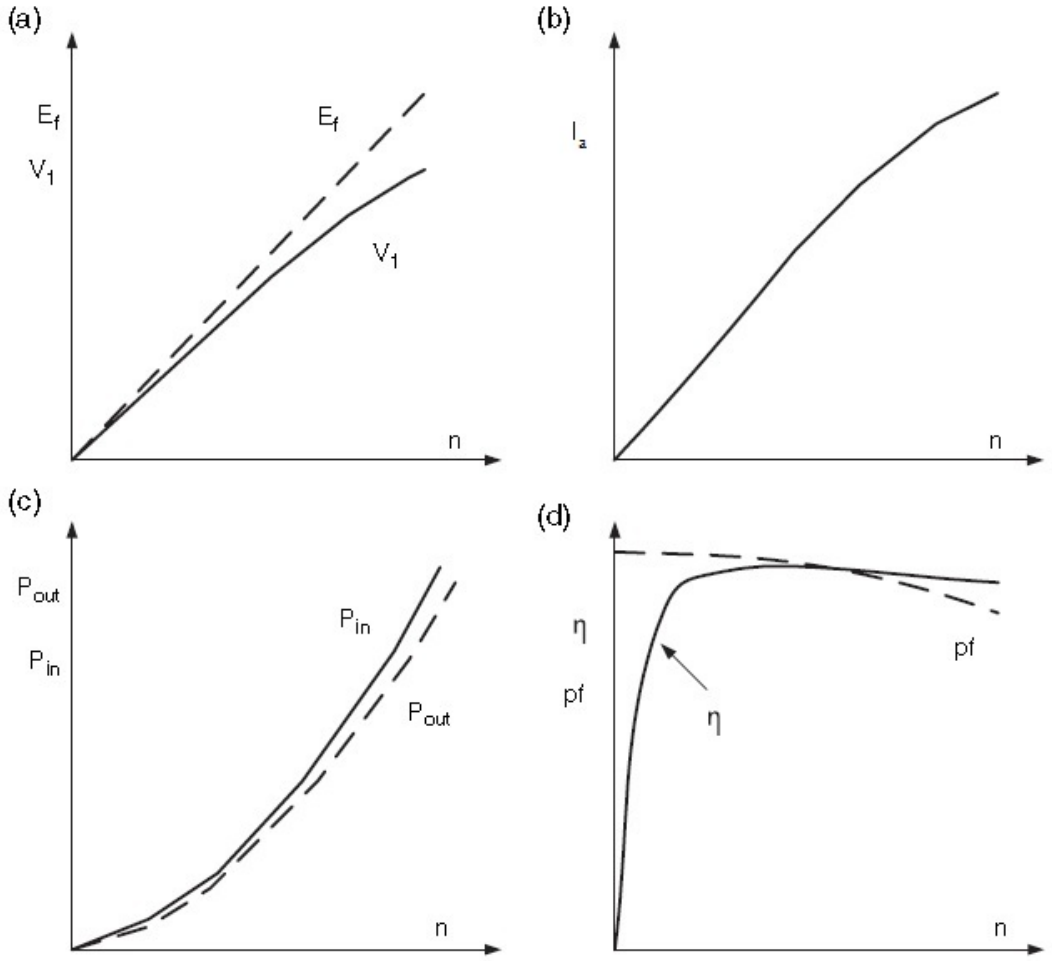

Figure 2.28: Characteristics of a stand alone AFPM synchronous generator for inductive load: (a) EMF E_f per phase and phase voltage V_1 versus speed n, (b) load current I_a versus speed n, (c) output power P_{out} and input power P_{in} versus speed n, (d) efficiency η and power factor $pf = \cos\phi$ versus speed n. [20]

2.3 Low-Power Electronics

2.3.1 Introduction

A well-structured scheme of low-power electronics is inevitable in converting and stabilizing the achieved power. Depending on the used kind of generator and turbine, other structures will be installed. Essentially, the electronics shall in our case, convert the generated electrical AC voltage to usable electrical voltage for battery storage, being DC power. The obtained voltage is therefore rectified by a DC rectifier. Subsequently, both input and output impedances, being the generator impedance and a battery charger, should be matched. An adequate converter converts this voltage then to the correct voltage level for feeding the charger. Eventually, the DC battery voltage may be inverted again to AC and to another magnitude, depending on further needs of connected loads.

2.3.2 Rectifiers

Basic Rectification Principles

A rectifier basically converts AC voltage to DC voltage. The simplest rectifier is a single-phase half-wave rectifier, consisting of a diode D, a resistive load R and a sinusoidal AC voltage source. Assuming that all components are ideal, figure 2.29 shows a fundamental rectifier circuit of a single-phase half-wave rectifier with a resistive load. The AC source is represented by an AC source $v_s = V_m \sin \omega t$ and a transformer, and v_m is the maximum peak voltage. v_D represents the voltage across the diode and v_R is the voltage across the resistor. The diode conducts for half of the period, which is the case when the voltage signal rises above 0. An electrical current i_L flows in the circuit and varies sinusoidally. From the moment the source voltage becomes 0 again, the diode starts blocking and the *peak inverse voltage* (PIV) will prevent the circuit of conducting electrical current. Important is that when this PIV becomes to big, a break-down or "avalanche" of the semiconductors may occur. This maximum voltage that the semiconductor shall withstand is called the *peak repetitive reverse voltage* (V_{PRR}) and must be considered in the selection of a suitable rectifier. Hence, half of the period, when the diode conducts, the source voltage drops across the resistor, and half of the period, when the diode is blocked, the source voltage drops across the diode. On figure 2.29, corresponding graphics are shown, representing signals of v_s, v_L, v_D and i_L [23].

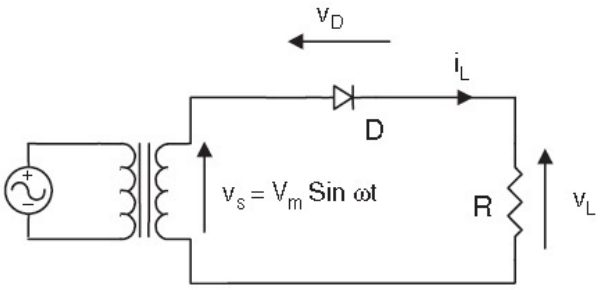

Figure 2.29: Single-phase half-wave rectifier with resistive load [23].

As is represented on figure 2.30, for a half-wave rectifier only for half of the period an output voltage is obtained. This consequent drawback decreases the output voltage substantially and may be solved easily combining two half-wave rectifier circuits, such one takes care of the positive, and one for the negative alternation. Thus, a full wave rectifier is achieved, and two different full-wave types can be distinguished. One example is a full-wave rectifier with a center-tapped transformer, which is represented in figure 2.31. Here, the central tapping on the transformer splits the source voltage up in two equal parts, both represented as V_S. The PIV voltage is doubled for both diodes D_1 and D_2, as shown on the graphics of figure 2.32. The peak repetitive reverse voltage therefore has to be doubled as well [23].

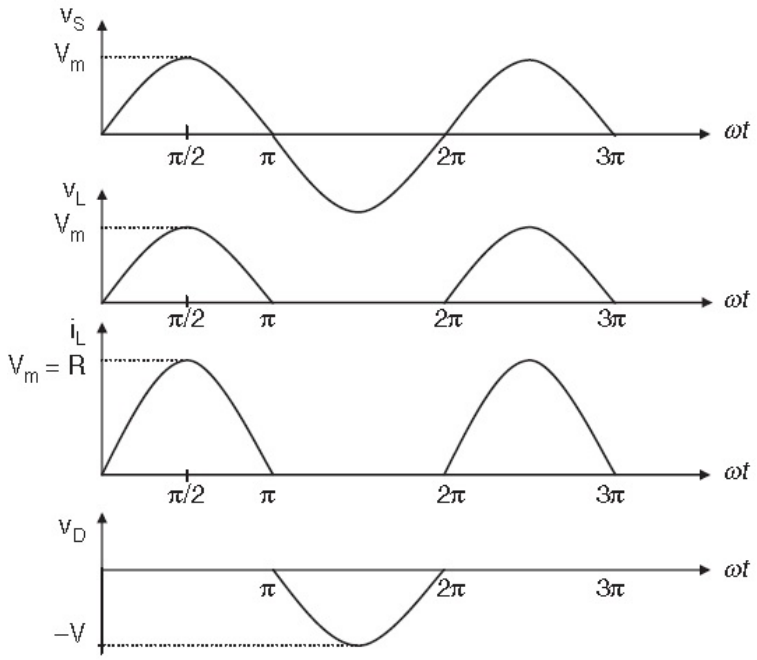

Figure 2.30: Voltage and current waveforms of the half-wave rectifier with resistive load [23].

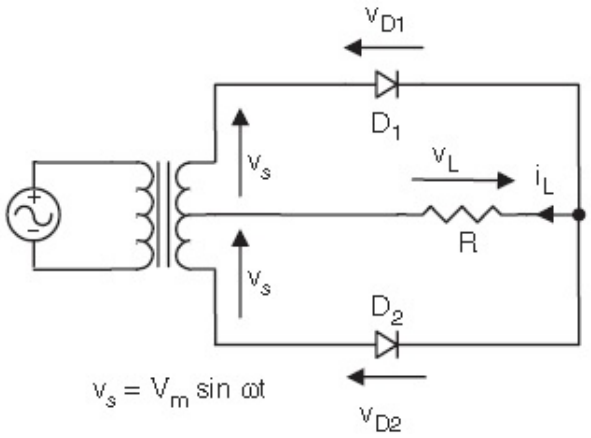

Figure 2.31: Single-phase full-wave rectifier with a center-tapped transformer [23].

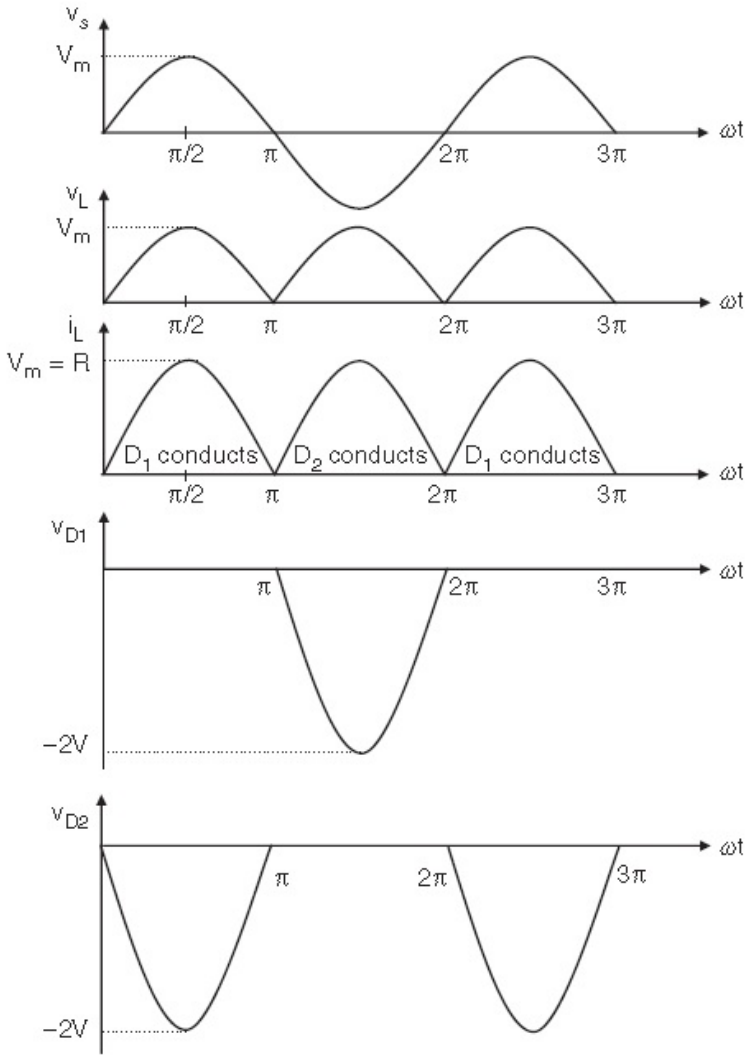

Figure 2.32: Voltage and current waveforms of the full-wave rectifier with a center-tapped transformer [23].

This latter undesirability can be solved using a second type of a full-wave rectifier, a bridge rectifier. An electric circuit of this is shown on figure 2.33 and waveforms are shown on figure 2.34. Four diodes D_1, D_2, D_3 and D_4 are used, where two diodes for each phase are placed in series, so that this previously doubled voltage can be divided over two diodes per phase. Disadvantageously, the forward biasing voltage drop doubles as well [23].

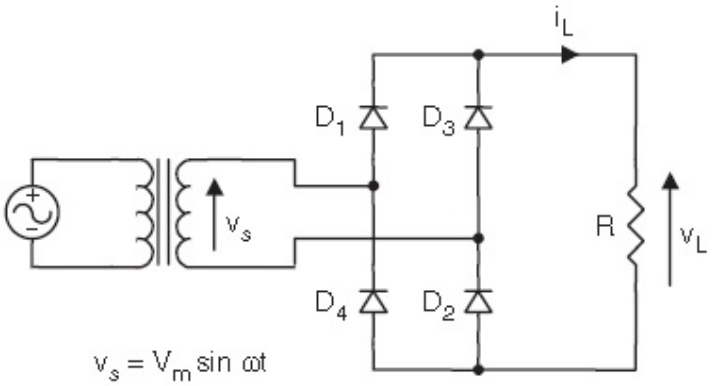

Figure 2.33: Single-phase bridge rectifier [23].

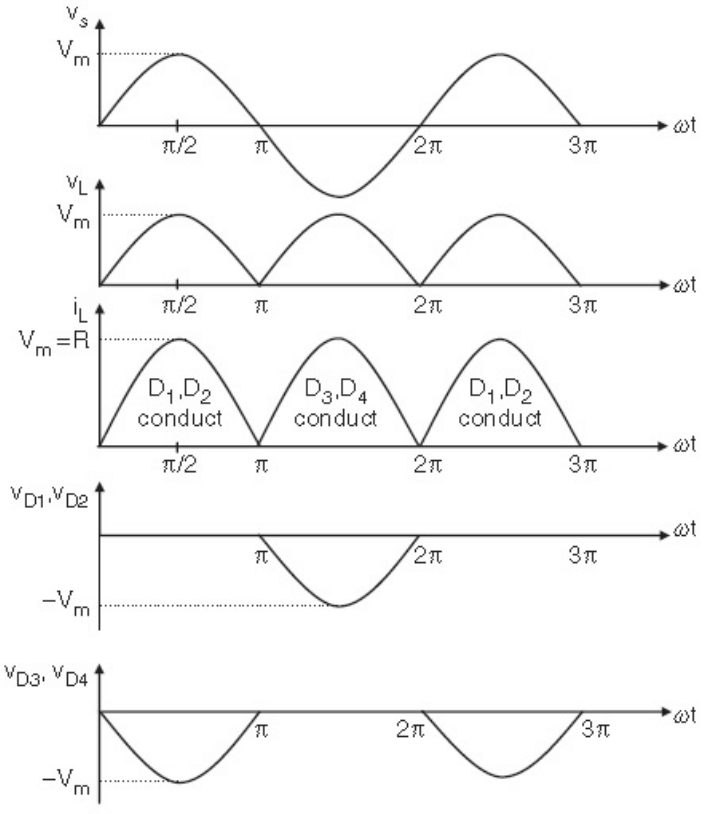

Figure 2.34: Voltage and current waveforms of the bridge rectifier [23].

Three-phase rectifiers can be understood easily using the same rectifying methods for three different phases. Passive and active filtering can also be separated as will be explained further in this chapter.

Filtering Methods for Rectifiers

A rectifier simply converts AC voltage into a positive alternating voltage. Therefore, a filter is necessary to obtain a flattened DC signal. The easiest way for doing this is by passive filtering, using an additional capacitor or inductor. A capacitor can store energy as an electrical charge, which may retaliate the voltage variation when being placed parallel across the output resistor. A scheme of a full-wave rectifier with a capacitor as input DC filter is shown on figure 2.35. When the instantaneous source voltage is higher than the instantaneous capacitor voltage, the capacitor starts charging, when vice versa the source voltage is lower, both diodes are blocked and the capacitor starts discharging through the load resistor R, resulting in a smaller ripple voltage. This so-called *ripple* is the difference of the maximum and minimum output voltage, as shown on figure 2.36, where $V_{r(pp)}$ represents the peak-to-peak ripple voltage. Consequently, the diodes conduct for shorter periods as in case of no filtering. This phenomenon may be expressed by a conduction angle θ_c, which decreases for smaller output ripple voltages. In case of using an inductor, this element should be placed in series with the load resistor. Results are similar as for a capacitor, but energy is stored here in a magnetic form [23].

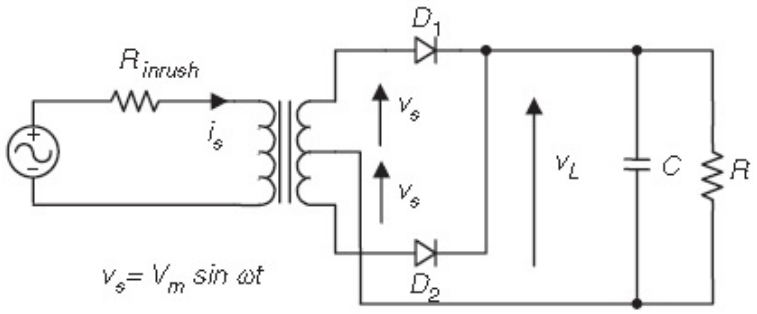

Figure 2.35: Full-wave rectifier with capacitor input DC filter [23].

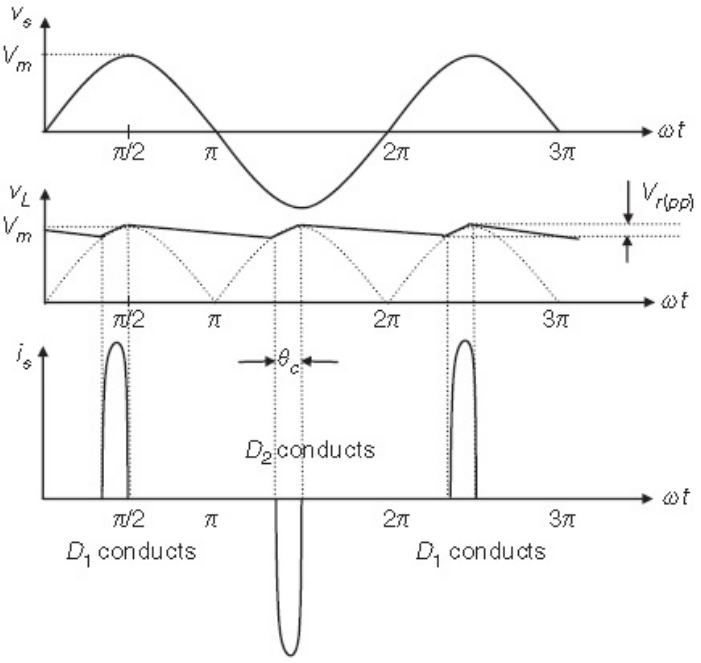

Figure 2.36: Voltage and current waveforms of the full-wave rectifier with capacitor-input dc filter [23].

Dependent on the used capacitor, a ripple will remain in the output signal, which can be expressed in a ripple factor (RF). For explaining this factor some other parameters should be explained first. V_{dc} is the average of the load voltage v_L and is similar to the DC component of this voltage [23]:

$$V_{dc} = \frac{1}{T}\int_0^T v_L dt \tag{2.15}$$

V_L is the rms value of the load voltage v_L:

$$V_L = \sqrt{\frac{1}{T}\int_0^T v_L^2(t)dt} \tag{2.16}$$

And the AC component V_{ac} can be found as the effective or root mean square (rms) component of the AC voltage component, which is equal to the rms value of v_L minus the DC component of V_{dc}:

$$V_{ac} = \sqrt{V_L^2 - V_{dc}^2} \tag{2.17}$$

An equation for the RF can finally be expressed as the fraction of the AC component of the voltage V_{ac} to the DC component V_{dc} and can be simplified using previous equation 2.17:

$$RF = \frac{V_{ac}}{V_{dc}} = \sqrt{\left(\frac{V_L}{V_{dc}}\right)^2 - 1} \tag{2.18}$$

Furthermore, active and passive filtering can be considered. Passive filters have no actively regulated semiconductors. MOSFETS and thyristors are examples of this because their output power can be controlled by alternating the phase angle which is controlled using *pulse-width modulation* (PWM). In PWM the average value of voltage (and current) fed to the load is controlled by turning the semiconductor switch on and off at a fast rate. The longer the switch is on compared to the off-periods, the higher the average will be. By changing the frequency of alternation, signals can consequently be adjusted to what is needed. Additionally, passive filtering can only be used for low frequencies and no regulation is furthermore possible [24].

2.3.3 Converters

Power production varies in time for our underwater vehicle. Depending on the velocity of the water stream, the produced AC voltage varies in frequency. The magnitude of this voltage varies consequently to the water force. This is what we call a *wild* AC output. Hence, this alternating AC voltage is not perfectly sinusoidal, and a lot of different frequencies may occur. In contrast to large-scale grid-power production, for which in Europe a frequency of 50 Hz is manipulated, a range of workable frequencies can be defined here. Since batteries only charge for voltages higher than the already stored voltage, a voltage converter is inevitable. This converter shall be controlled by low-power electronics, tending a constant and converted output voltage, irrespectively of how external conditions might be. A buck and a boost converter can be separated here. Buck converters decrease the obtained input voltage to a lower level, whereas boost converters increase this level. Since the achieved voltage is scarce and batteries normally require higher voltages, a boost converter is most likely in our research.

Boost Converter

In figure 2.37, a basic scheme of a boost or step-up converter is represented. V_s is the DC voltage source, L is the boost inductor, S is the controlled switch, C is the filter capacity and R is the load resistance. On figure 2.38 the waveforms can be observed. When the switch S is in the on-state, meaning that it is closed, a short circuit is formed through the inductance L and energy is stored magnetically. If the switch is in the off-state, or opened, the current i_L flows through the diode for which also the stored energy is released through the diode. Thus, both the source and inductance energy flow in this case through the diode. The capacitance flattens the discontinuous output to a continuous signal by charging and afterwards decharging through the load. As the name suggests, the output voltage is here higher than the input voltage [23].

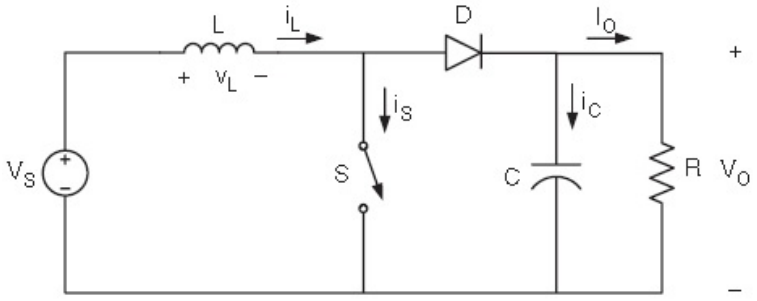

Figure 2.37: Boost converter [23].

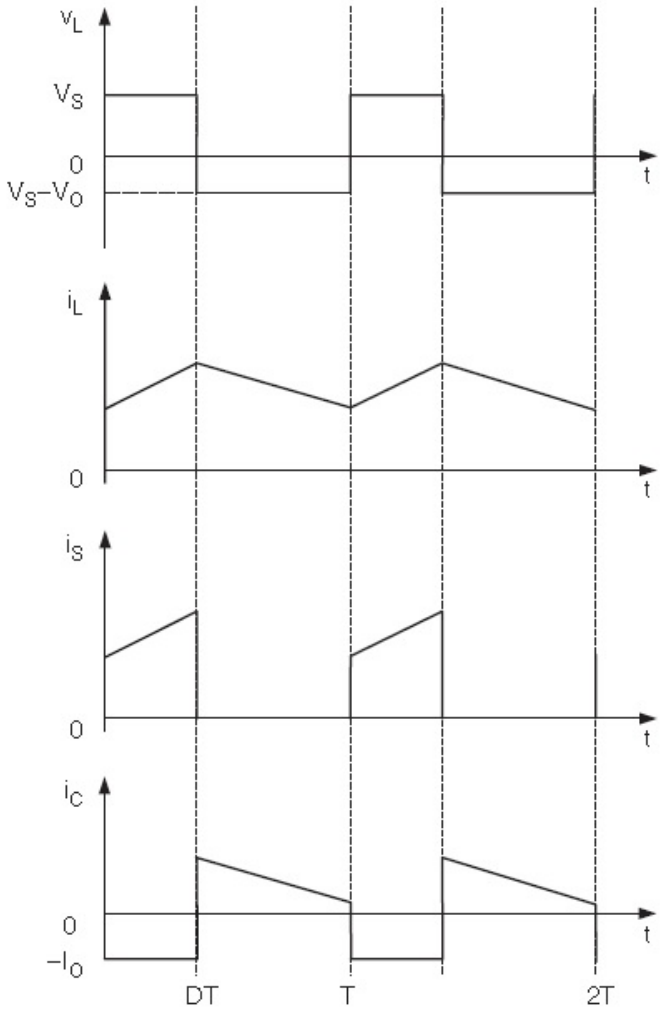

Figure 2.38: Waveforms of boost converter [23].

Performance of Boost Converter

One important factor for all the electronics, is retaining a high efficiency. To make this the highest as possible, all component parameters shall be optimized. The duty cycle (δ) of a signal is the periodic time percentage that a signal is high, hence the time that a switch of a converter is closed compared to the periodic time that a switch is closed and opened again. Pulse-width modulation is, in case of converters, the alternation of the time that a switch is closed, respectively opened, to change the ratio of the input to the output voltage. The frequency represents here how often this signal is reshaped.

According to [25], results of approximately 96% were found for a prototype boost converter, for duty cycles of 0.80. The PWM frequency of the signal was set up to 36 kHz. On the output, a 500 Ω load resistor was connected. Thus according to the graphics on figure 2.39, we can conclude that if the duty cycle increases, more current is induced in the boost converter circuit, and copper losses may increase consequently. Logically, efficiency of the converter decreases for higher currents by reasons of Joule's law and by other phenomena as e.g switching losses of MOSFETS and so on.

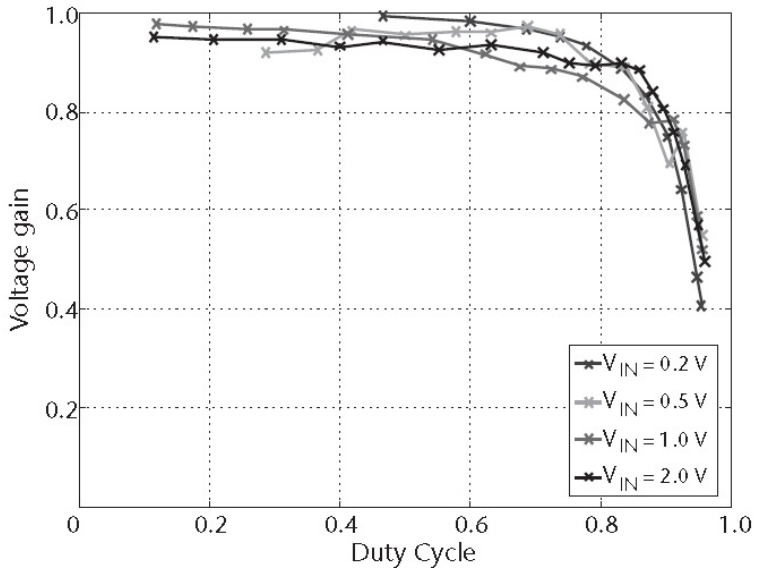

Figure 2.39: Results of experiment proving decrease of efficiency for increasing duty cycle [25].

Buck Converter

A buck or step-down converter is meant to do the opposite, and decreases the output voltage. A schematic and its corresponding waveforms are shown on figure 2.40, respectively figure 2.41, assuming that the inductor current is always positive. When the converter operates in the on-state, the diode is blocked and current starts to increase from zero on. Hence energy is stored again in the inductor. This energy is released when the converter continues to the off-state and the current flows through the diode. The power source is then disconnected. For what a lower output voltage is obtained than seen on the input.

2.3.4 Possible Semiconductors

As semiconductors are not perfect, a voltage drop emerges, which decreases the output voltage of the circuit. Silicium diodes typically deal with a theoretical voltage drop of about 0.7 V, when being forward biased. For Schottky diodes, this is only 0.15 to 0.45 V. Thus, scarce generated underwater voltage can remain more usable, for which the output power efficiency improves. Furthermore, Schottky diodes also have faster switching frequencies than Silicium diodes. This characteristic is extremely useful because of the previous mentioned wild AC output, for which frequency and magnitude may vary. Hence, the elementary electronic components, have to withstand these higher ranges of both frequencies and peak voltage values.

Furthermore, also active and passive semiconductors can be separated. Passive components as diodes do not require any control but provoke a constant voltage drop due to the forward biasing of the elements. Active components are controlled by which this voltage drop can reduce. Since our generated voltages are estimated to be low, decrease of the forward biasing voltage drop might result in a substantial efficiency improvement. Examples of active components are MOSFETS and thyristors. MOSFETS are used more and more because of this lower voltage drop and an according higher efficiency. Another advantage of the MOSFET is the fast recovering time, which makes them more usable for fast switching applications remaining high in terms of efficiencies. Thus, MOSFETS are recommended in low power applications and are enormously useful in rectifier and converter circuits as semiconductors and switching gates.

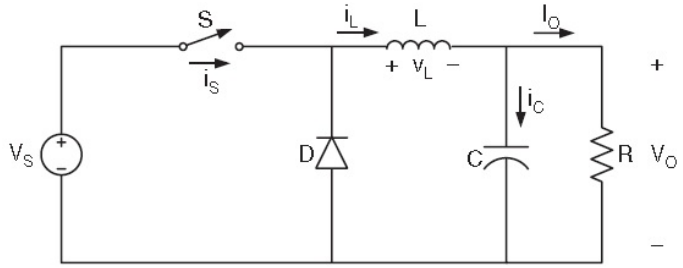

Figure 2.40: Buck converter [23].

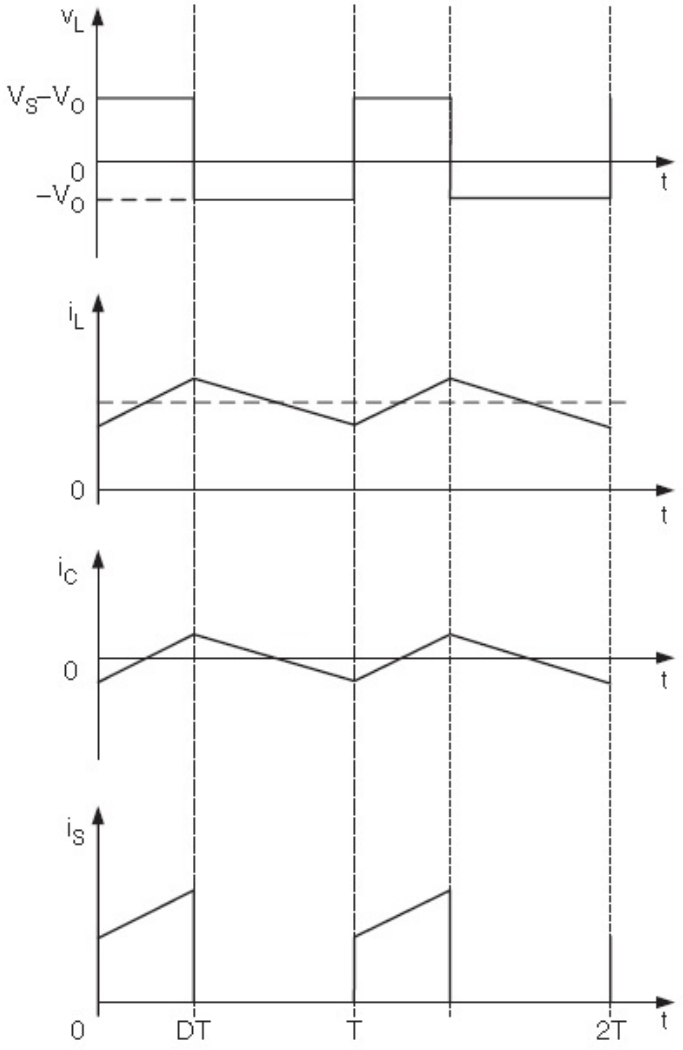

Figure 2.41: Waveforms of buck converter [23].

2.3.5 Matching Input to the Output

One of the most important things, using low-power electronics, is to set an adequate match between the input and the output impedance [25]. If not, power transition will not be optimal and efficiency might reduce substantially. Although, as was already briefly discussed in the introduction, a difference exists between maximum power and maximum efficiency. Since no cost is directly related to the amount of harvested energy, efficiency is important, but overall maximized power achievement is of primary importance. Moreover, for a maximal efficiency, the load resistance R_{Load} should be significantly larger than the source resistance R_{Source}, ensuring most of the power is consumed by R_{Load}, instead of R_{Source}. For a maximal power transfer in contrast, R_{Load} should be equal to R_{Source}, for which the overall resistance of the two becomes the lowest. Hence, a higher current, and correspondingly a higher power transfer is achievable. Both these generalities are drawn on figure 2.42.

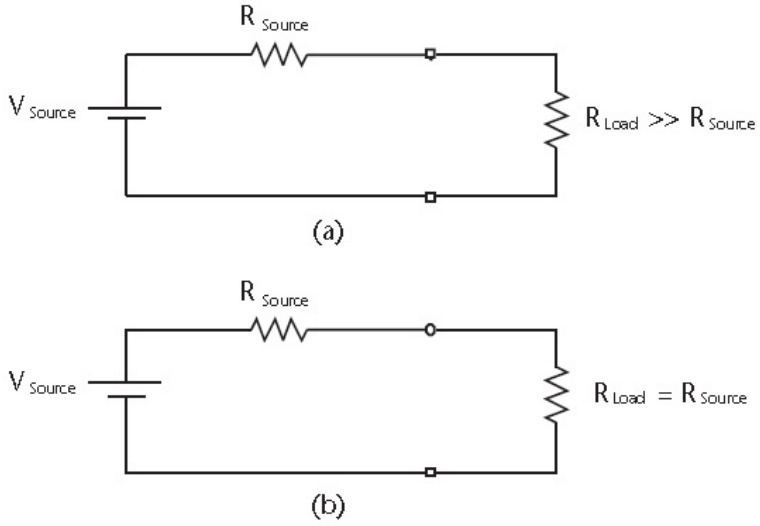

Figure 2.42: Maximum efficiency of energy transfer to load [25].

However this example provides a reasonable solution, assuming a simple and constant resistive load, our system tends to feed a battery charger. Thus, consequently the load resistance may not be constant over an undefined range of time. A control unit has to overcome variations of this resistance, pursuing a permanent optimal match between input and output.

2.3.6 Losses

To achieve a maximal power conversion, losses should as much as possible be avoided. In order to pursue this optimum, components should be efficient, but also superfluous elements should be omitted to simplify circuits and to reduce the component number. A first well known loss is the electrical conduction loss caused by Joule's law. Additionally, in case of considering active low-power MOSFETS, the charging process of the gate capacitance should be involved. Consequently, due to inertia switching losses caused by pushing charge on and off the gate of MOSFETS, also efficiency is influenced disadvantageously. Further, for diodes the forward biasing loss should be encountered for which this loss is mostly higher than in case of active components.

2.3.7 Combined Circuits

Benefits

The lower the acquired voltages are, the more critical the reduction of losses becomes. Therefore, in micro-scale energy harvesting this is decisive to guarantee the highest efficiency as possible. Executing a rectifier and a step-up capability as one single module, for which one or more electronic parts can be excluded, is here a first improvement. As well, the component size will decrease correspondingly to this. Reducing the number of transmission steps of the electronic process (by combining circuits), results into simpler designs, which is in favour of the overall efficiency. Several harvesting techniques involve adjusted techniques for harvesting energy at voltage levels in a range of a few microvolts to a few tens of milivolts. Extrapolating these used principles to higher power levels of a few volts can therefore be interesting, but requires a careful study. In case that extreme low voltages are considered, an electromechanical *transducer* or a low-power generator is inserted to induce the necessary voltage. Generators designed for low voltages as a few milivolts are in this case not rare. Many other types of transducers are designed, as is clearly explained in [25].

Full-Wave Center-Tapped Transformer Configuration using Schottky Diodes

Interfacing an electrical transducer to a battery charger, requires rectification, step-up capability and impedance control. In a first practical model for harvesting low voltages, Schottky diodes are used as semiconductor elements. Since they resist higher PIV'es, they can be mounted as a full-wave rectifier with a center-tapped transformer. Clearly, forward biasing voltage drop is therefore only half of the bridge emplacement. The center-tapped transformer upconverts the

low voltage to a higher level, therefore a complex converter circuit is superfluous. A capacitor is coupled to the output to flatten the rectified signal. Although this configuration meets the first two requirements, no appropriate impedance match between the generator and the interface electronics is accomplished, thus power transfer is not optimal. A benefit of this emplacement is the frugal use of electronic components preventing unnecessary losses and chances of fatal breakdown. As well a step-up possibility is fulfilled in an easy way [25].

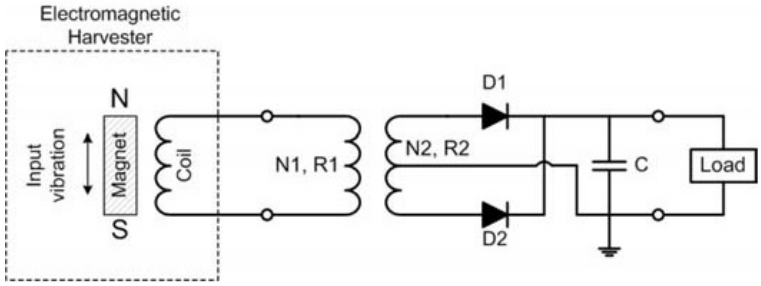

Figure 2.43: Full-bridge center-tapped transformer configuration, which performs voltage step-up and rectification, using two Schottky diodes, a transformer and a filter capacitor [25].

Villard Voltage Multiplier

By reasons of avoiding magnetic components, as transformers, a Villard voltage multiplier circuit was developed. As marked on figure 2.44, for every block of two diodes and two capacitors, the voltage is doubled, attaining easily voltages of several thousands of volts. However, a sufficient impedance match is still not fulfilled properly, and thus neither this circuit can be used for optimal power transfer [25]. One application for which these exacting requirements are crucial are high energy physical experiments.

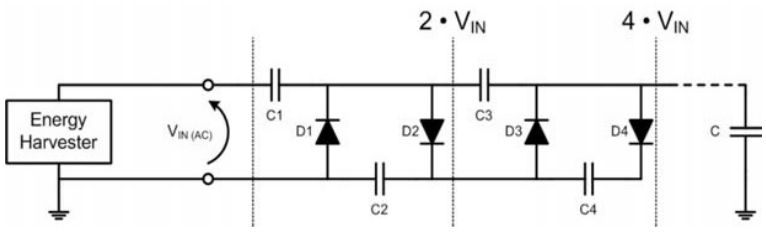

Figure 2.44: Villard voltage multiplier [25].

Dual-Polarity Boost Convertor

To solve the impedance match, the dual-polarity boost converter circuit is designed. Here, rectification, impedance match and voltage step-up are executed as one circuit. An impedance match is achieved between the generator's internal resistance and the load. This circuit provides a low-voltage rectification of both positive and negative half-cycles. Two separate boost converters are activated alternatively by the pulse modulator, for rectifying and upconverting the AC signal. Moreover, the dual-polarity of this type eliminates the need for an external diode-bridge rectifier. As well, the circuit fulfils the step-up requirement equally as a normal boost converter circuit does. Synchronously switched MOSFETS or Schottky diodes are recommended by the author, for the sake of reducing power losses [25].

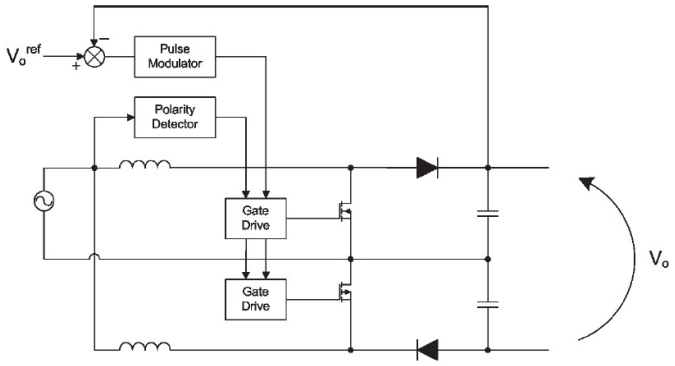

Figure 2.45: Example of dual-polarity boost converter [25].

Adaptive Impedance Matching using Switched Capacitor Arrays

Involving switched capacitor arrays may be an alternative solution. Here, a capacitive voltage divider is proposed. Both arrays have the same capacitance, leading to an equal source voltage division across both arrays. An appropriate impedance match between the generator's internal resistance and the load is consequently achieved. Both arrays are switched alternately in charging, respectively discharging modus. Here, the capacitor arrays are first charged to a maximum voltage of $0.5V_{gen} + \Delta V_{charge}$ during a charging time t. Then, a switch toggles to the other state so that the charge is connected to a storage capacitor C_b to discharge. This latter storage capacitor may then be connected to an attached boost converter, as further needs require. The capacitor array can additionally be discharged to a minimum of $0.5V_{gen} - \Delta V_{discharge}$. Depending on the allowed value of ΔV, a switching frequency can be defined. Power losses may decrease using this system.

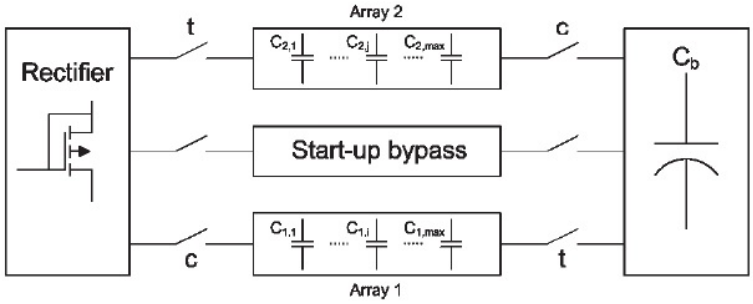

Figure 2.46: Adaptive impedance matching technique using switched capacitor arrays [25].

2.3.8 Input Impedance Control

Changing power availability caused by external conditions and different power requirements from the battery side, results in an adequate control strategy. In this report, and as requested, the load is limited to the battery charger. The resistance of the input of the boost converter R_{in} is adjusted actively to the output or load resistance R_{load} by alternating the duty cycle. A general equation which represents the boost converter resistance conversion is the following [25]:

$$R_{in} = R_{load}\left(1 - \delta^2\right) \tag{2.19}$$

On figure 2.47, a schematic flow chart is represented, showing a conceptual implementation of a possible impedance match for a boost converter [25]. The boost converter current, $I_{measured}$ can be measured using a sense resistor R_{sense} and a sense amplifier. A sense amplifier converts the current to a proportional voltage for use in the microcontroller by making use of the sense resistor. This resulted signal can here be compared to a demanded value, obtainable as the input voltage of the boost converter $V_{in,boost}$ divided by the armature resistance of the generator R_{arm}. The proportional and integral (PI) compensator can calculate afterwards an optimal duty cycle, and adapt the frequency of the boost converter switch in order to achieve the least possible error current I_{error}. Thus, a near perfect impedance match is achieved between the generator armature resistance and the equivalent load resistance that the generator sees.

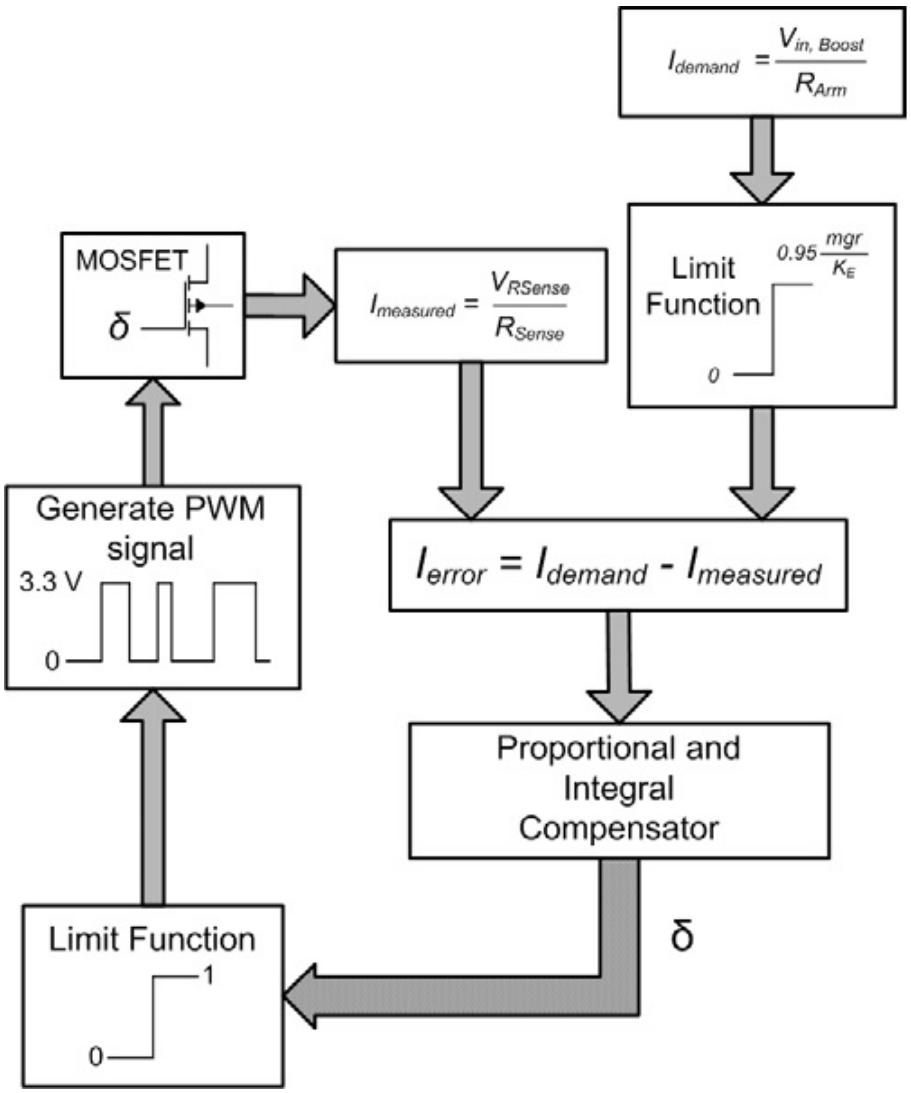

Figure 2.47: Flow chart of the boost converter input impedance matching procedure [25].

2.3.9 Overall Topology using Boost Converter

Figure 2.48 represents an overall block diagram of the power processing and the corresponding control circuitry for implementing impedance matching [25]. The power source is simulated by a DC voltage and an equivalent source resistance. This voltage is converted to a higher level by a boost converter which is programmed as impedance matching unit. A microcontroller fulfils a PI compensator role and samples the boost converter input voltage V_{in}, inductor current I_L and the voltage across C_{store} for comparing the input to the output impedance and adjusting this to a correct proportion. In fact a closed-loop composition is created, in order to obtain feedback signals and to adjust deviations of the desired and calculated value. It reads that the duty cycle is calculated according to the matched value of the impedances. This regulated duty cycle is reflected by pulse-width modulation at the MOSFET switch of the boost converter, and is correlated to the impedance proportion expressed by equation 2.19. Thus, this converter sets the variable voltage to a fixed level and regulates an optimal power flow for every power level between a convertible upper and lower limit. The supercapacitor C_{store}, accumulates energy and stabilizes the output voltage of the boost converter by filtering the remaining ripple. Finally, a buck converter is installed in this case to convert the supercapacitor voltage to a constant output level according to the load's needs.

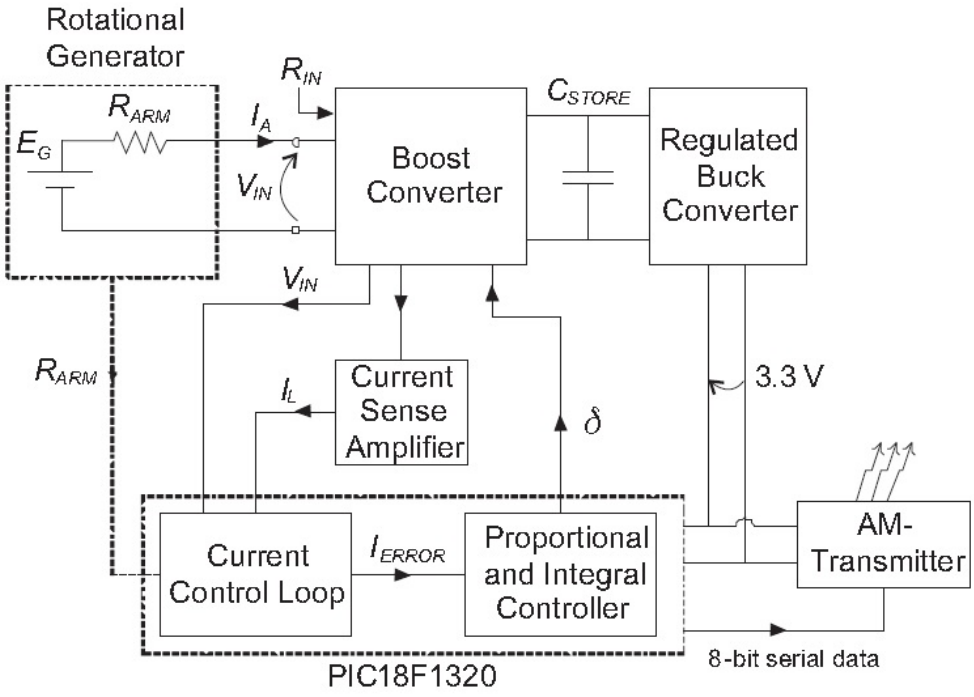

Figure 2.48: Overall topology for impedance match between input and output [25].

In this case, e.g. three series-connected supercapacitors of 6 mF, rated at 15 V, are used as voltage storage element. Also, an off-the shelve buck RECOM regulated buck converter with a vast input range of 4.75 V to 34 V and a regulated output of 3.3 V is connected. A PIC18F1320 microcontroller was used for PI controlling and to achieve the demanded output of 3.3 V for the AM-transmitter load.

Chapter 3

Project and Requirements

3.1 TURTLE

TURTLE is a recently launched project involving many people and meeting several goals. The objective of this project is to develop a prototype of an underwater vehicle. A three-dimensional sketch of how this structure is supposed to look like is shown in figure 3.1. Several additions, like a longer presence at seabed are incorporated for which new robotic ascent and descent energy efficient technologies are inevitable. This prototype could be used by both civilian and military stakeholders for underwater operations to explore seabed, and at particular benthic depths that require advanced technologies for which automation of operation and increased efficiency are the most important key factors. Several sensors and cameras are implemented to obtain all data that are necessary for the performed researches. A general CPU is the central control unit of the vehicle and performs all the complete operation of the vehicle. Several thrusters, together with a variable buoyancy system are responsible for relocating the system. A pump fills a tank with water under pressure to adapt the buoyancy of the vehicle and to facilitate ascent and descent movements. Additionally, a block of flotation material, mounted on top of the vehicle, decreases the general buoyancy. Communication is provided using GPS, Wi-Fi and radio signals that are transmitted by antennas between the vehicle, an on-the-spot buoy to localize the underwater vehicle and a ground station where staff can retrieve the vehicle's data. Thus, in fact, communication occurs between the underwater vehicle and the ground station with the help of a buoy to localize the vehicle using acoustic signals and all control is executed automatically inside the vehicle. The structure of TURTLE is represented in an overall block diagram and a sketch of how this structure might look in practice (figure 3.3 and 3.2) [27].

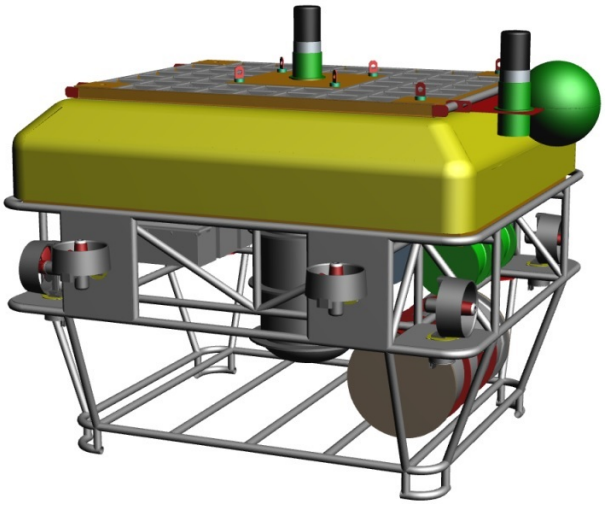

Figure 3.1: TURTLE 3D sketch.

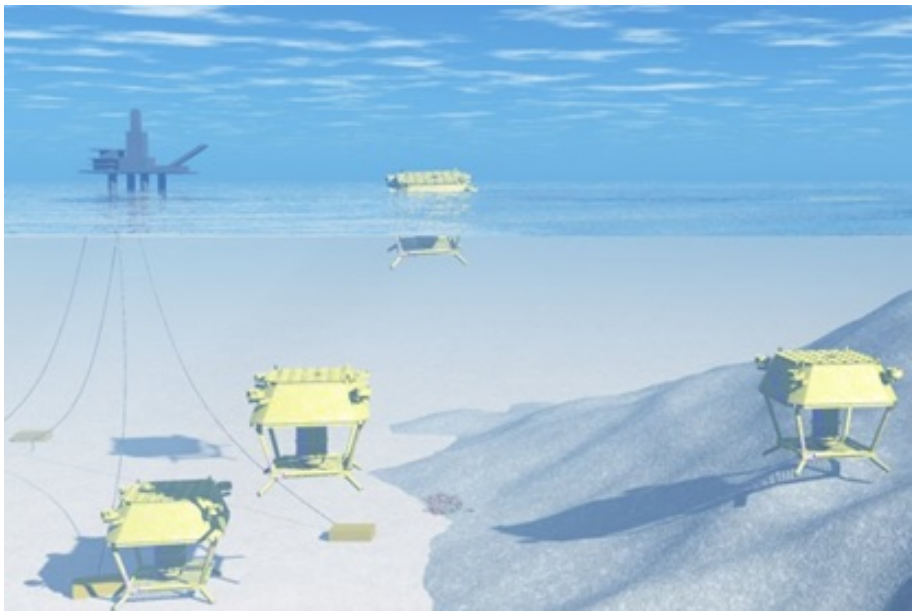

Figure 3.2: TURTLE simulated operation.

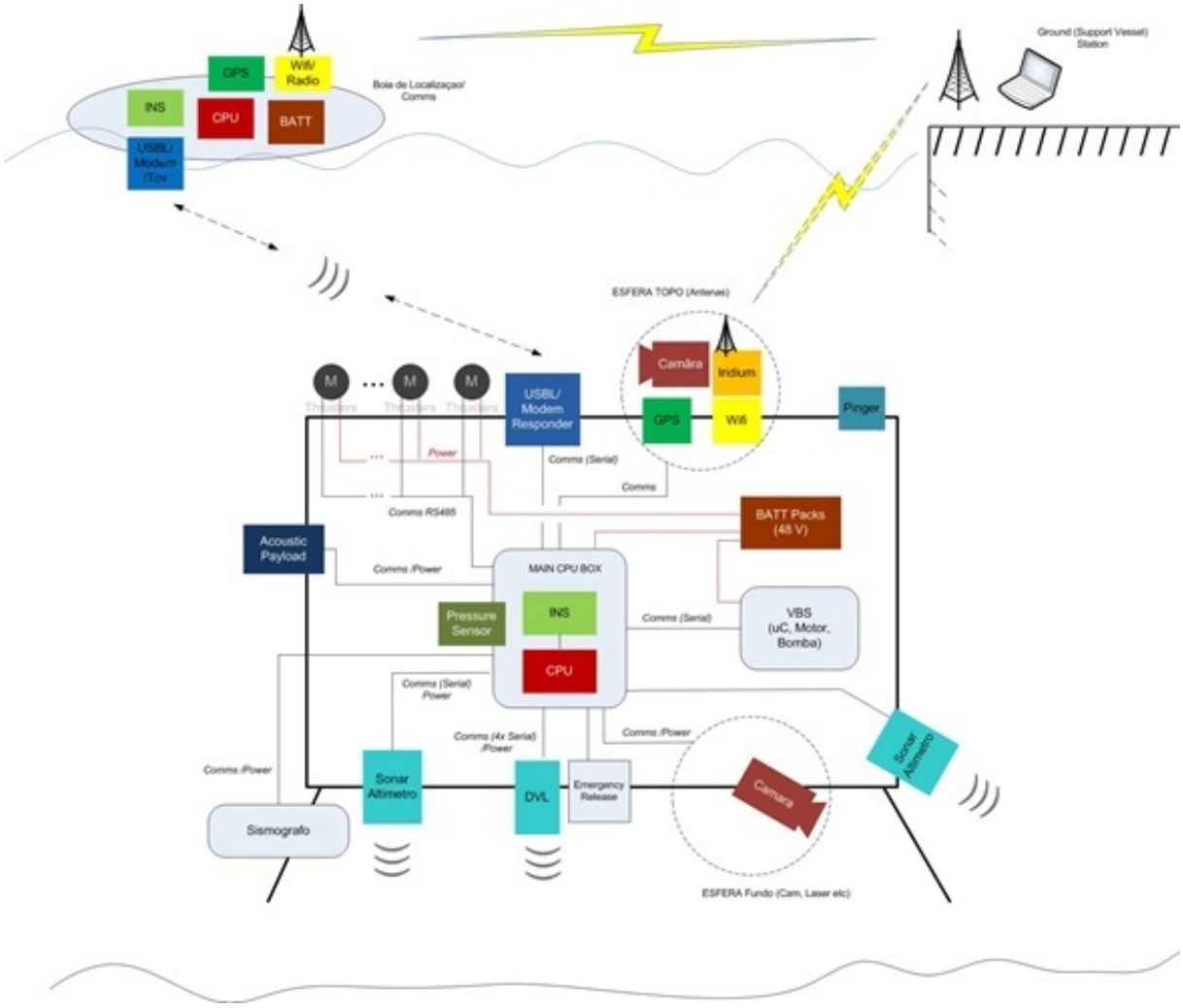

Figure 3.3: TURTLE component block diagram.

3.2 Energy Supply

Proper operation of vital components is of substantial importance in a delicate vehicle as TURTLE. On figure 3.4 a schematic of the vehicle's electrical structure is outlined. A mechanical torque is induced by the turbine, which is transformed into an electrical torque, which is in turn converted to the correct output voltage by the low-power electronics for feeding a battery charger. The charger subsequently controls the voltage to an adapted level depending on what the battery charging cycle on that moment requires. Consequently, the charger controls the battery power by limiting the current to a maximum level, in order to prevent overheating of the cells. Current can easily bypass battery cells when the cells are completely charged, using a good control strategy of the charger. When all loads are additionally fed, remaining current is consumed by a dump load.

A priority according to which component should be fed first should be set up. The CPU of the system is programmed such an adjusted load is chosen correspondingly the amount of energy that is available. Vital components as e.g. communication systems and the proper CPU should in any case be fed. If not, the vehicle is impossible to control and might get lost. Subsequently, secondary loads as thrusters, sensors, cameras and so on, might also be connected to the provided energy supply. Although, other related studies describe the power distribution of the TURTLE, the idea in this work is only to describe the feeding of the battery charger, no matter how the power is distributed for different loads. It reads that the load is moreover an independent unit and is therefore assumed to be irrelevant for charging the batteries. As encircled on the diagram of figure 3.4 we delimit the examined structure for this paper to the turbine, generator and low-power electronics. For these three blocks we will define an implementable structure in chapter 4, by which we will keep in mind that this power is for feeding the battery charger.

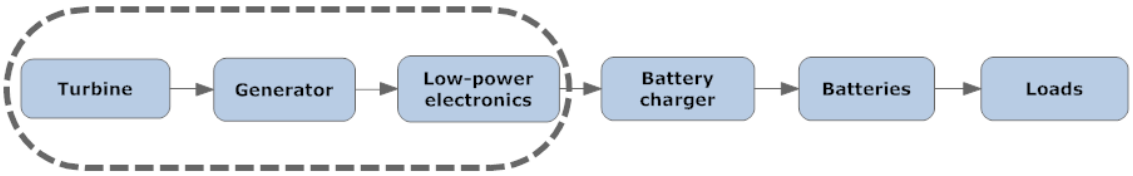

Figure 3.4: Electrical block diagram of TURTLE.

3.3 Requirements

Some specific requirements should be considered to ensure proper operation of the TURTLE energy system:

- Water velocities are expected to be between 0.1 and 0.5 m/s. Proper energy harvesting can therefore only be guaranteed in this interval. For lower velocities, induced lift and drag is not ensured being able to overcome the mechanical and electrical counteracting torque of the system anymore. For higher velocities, the system might be damaged.

- The turbine blades cannot exceed the prototype's surrounding dimensions. The outer framework is rated to have a height of about 1.4 m, and a width and length of both 1.5 m. Hence, a maximum height and diameter of the turbine is rated at 0.8 m respectively 0.5 m. Based on equation 2.6, which defines the cross-section area of a cross-flow turbine, we can set this parameter at 0.4 m^2.

- To define margins for a feasible power interval, we have to consider equation 1.1 again. Adding in this formula the power performance coefficient C_P, and neglecting overall efficiency of the system, might lead us to the following formula:

$$P_T = \frac{1}{2}\rho A v^3 C_P \tag{3.1}$$

  Here we might add the aforementioned maximum velocity of 0.5 m/s and cross-section area of 0.4 m^2, and if we know that ρ is 1022 kg/m^3 and C_P is limited to $\frac{16}{27}$, a maximum power production of about 15 W is calculated. Additionally we can set a safety margin in case that higher water velocities would occur, and expand this limit to the previously set maximum of 30 W. Subsequently, we can set all different dimensions of the system components. Furthermore, if the supplied power comes too low, low-power electronics might no longer be able to overcome internal voltage drops of the semiconductors, for what power production will be excluded. Hence, defining this minimum requires additional experiments and calculations. If in contrast achieved power is too high, electrical components might overheat and eventually break down.

- The battery charger feeds 4 different battery packs (figure 3.5). Each battery pack consists of 16 in series connected battery packages, which in turn all consist of 4 different battery cells. In order to obtain an optimal charging cycle, all 16 battery packages are charged by a battery charger which requires 3.65 V input voltage for each of the 16 battery packages. Subsequently, the charger converts this supplied input voltage to a (varying) optimal charging voltage. This charging process is described in other related studies, and is therefore not further considered. Here, the only important requirement is that the charger needs 16 times 3.65 V at its input, which makes 58.4 V in total. In order to complete the picture, each of the 16 packages (which all contain 4 parallel connected battery cells) provide, if completely charged, a voltage of 3.2 V and 40 Ah (4 times 10 Ah). Thus, 16 battery packages each provide a voltage of 3.2 V (51.2 V in total), but all require 3.65 V each (58.4 V in total) from the charging unit, and provide a total capacity of 40 Ah. Eventually, this might be multiplied by 4 knowing that a combination of 4 battery packs is composed.

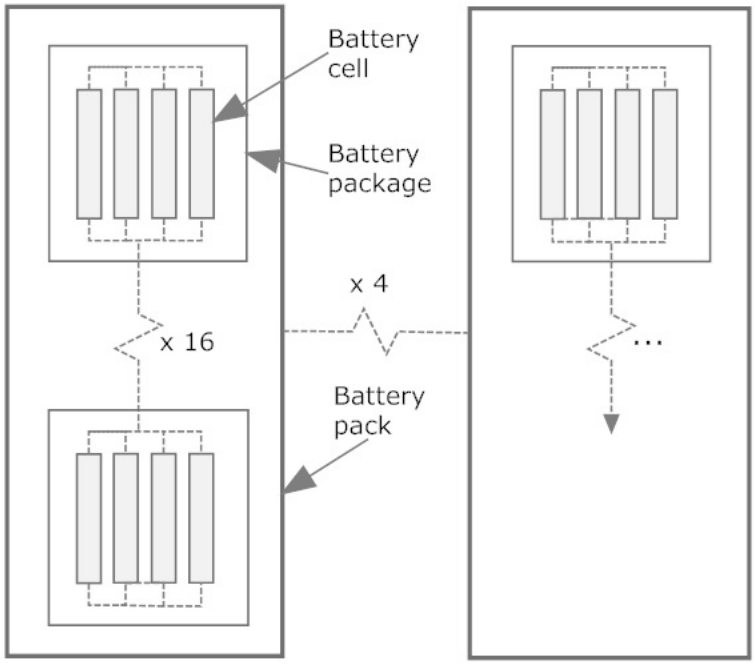

Figure 3.5: Sketch of the installed battery packs

- A pressure of about 100 bar should be considered for depths up to 1000 m. The turbine and other components exposed to this pressure shall consequently be designed of solid materials. Generators and electronics are normally not resistant against these pressures and should therefore be enclosed in a box to prevent direct contact with the water. At the place where this box surrounds the incoming shaft, an adapted high pressure seal should prevent water from penetrating. Optimizing this seal is beyond the scope of this work. The generator might additionally also be adapted such it can resist a high pressure, but this is not commonly executed so far.

- The energy system should be connected to the prototype's framework so that it can easily be removed by which no other elements are affected.

- Metal components additionally have to be chosen in order to avoid rust phenomena. Alloys of, among others, the turbine, shaft and interconnections should be adapted to prevent damage and eventual early break-down.

- Also unpredictable incidents as suddenly emerging high-velocity water flows, by which high voltages may be induced, should be prevented using a closed-loop electronic design that can block energy flow by chopping in the voltage when a critic level is reached.

Chapter 4

Analyses

4.1 Schematic Overview

A schematic overview of the electrical structure of the system is presented on figure 3.4. All three components shall be discussed separately in this chapter in order to find an optimum. The connotation of "optimum" refers in this case to a solution for which minimal power losses, feasibility, and simplicity in both implementation and use of components is pursued. The time for representing a theoretical solution was limited to three months. Because of this and also because the specific requirements were enormously restricted, and this study tends to develop a structure from which not any similar existing prototype has been developed so far, some ideas are combined together leading to an acceptable representation of a possible prototype. A completely unique solution could not be defined and is moreover irrelevant in this study. Influences of cost were additionally considered to be of secondary importance, thus efficiency results are not reduced by this. Our drawn structure might eventually, in a future study, be executed and upon which lots of tests could be done. Hopefully, this report might then be a good start for doing this.

4.2 Component Selection

4.2.1 Turbine

Based on several studies and comparisons of existing turbines [2, 7, 8, 15, 17, 10, 11], analyses can be performed observing the requirements. In this study, a vertical-axis cross-flow helical turbine is considered to be the better solution, for three main reasons:

- Turbine starting torque must in any case be ensured to exist. A helical type with a 100% blade wrap guarantees this requirement the most, having acceptable power results.

- Sweeping blades lead to a more constant torque curve compared to their straight equivalents (parallel to the axis). Mechanically, this results in a better self-start and a reduced shocking effect of blades, shaft, bearings, seals, etc. Correspondingly, lifespan of the components expands. The generator will additionally transform this torque into a more sinusoidal AC voltage, which is in benefit of the delicate low-power electronics that may see less harmonic values of the voltage in this way.

- A vertical-axis cross-flow turbine precludes water flow directionality the most, such a maximum torque induction is guaranteed the most. It reads that mounting the vehicle at seabed facilitates likewise.

Seeing our conditions, a commercially-available solution could not be found. Therefore, based on Niblick's results for which velocities between 0.4 and 0.8 m/s were examined [2], the following parameters should be set as described below while developing one's own turbine model. Because self-start is the main requirement of the turbine, first all parameters are set up in order to accomplish this. Later, when the actual turbine might be designed, a balance between a well-ensured self-start and optimal power results can then be found empirically.

- As outlined in chapter 2, the solidity ratio influences both the self-start and the tip speed ratio, and both parameters alter inversely proportional to each other. Thus, an optimum between both should be developed, however, as the self-start must be ensured in any case, a higher solidity ratio is preferred. This factor should be chosen higher than 0.3 for low velocities, and more specifically for velocities between 0.4 and 0.8 m/s, a solidity ratio is set up best between 0.3 and 0.4.

- The number of blades has been compared for different amounts and is directly proportional to the solidity ratio. Although, experiments comparing e.g. three and four-bladed types, resulted in a bigger static torque for the three-bladed turbine, as inertia is lower in this case, start-up is hence guaranteed to be more fluent for a three-bladed turbine.

- The pitch angle influences power coefficient and starting torque inversely. A smaller angle is considered to be better again, because of the easier self-start. Power coefficient will decrease. This declares also why a three-bladed turbine results in a better starting torque.

- Blade section should be set up big enough for ensuring a minimum lift force. If blades are not thick enough, water velocity of opposite blade sides differs not enough, and due to the Venturi effect expressed by equation 2.3, the differential pressure will also decrease.

- For lower aspect ratios, the starting torque shall improve. The power coefficient unfortunately decreases again for lower aspect ratios. Optimal power results may be obtained for a ratio of 12:1.

- The cross-section area is limited by the dimensions of the drawn prototype. This is also limited by reasons of deflection, vibration and stress on the blades. Therefore, the maximum height should be limited to 0.8 m and the diameter to 0.5 m, as was already estimated in chapter 3.

Finally, after contemplating all previous steps, a three-bladed turbine is still considered to be the best option. Dimensions of the cross-section area are set the highest as possible meeting surrounding dimensions. This is indicated in figure 4.1.

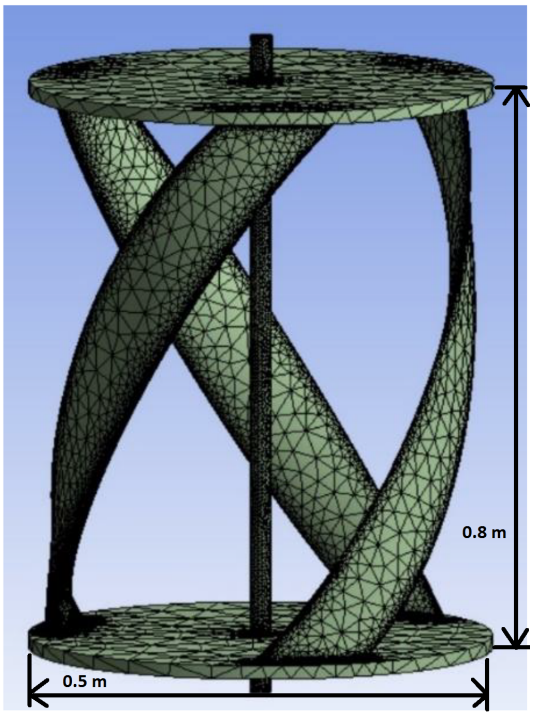

Figure 4.1: Three-bladed helical turbine [28].

Defining an optimal low-velocity blade profile, for which self-start and optimal torque induction is set up with certainty the highest as possible, is an immense complex study for which even calculations fall short. Developing this structure requires an elaborated study in itself provoking lots of experiments and simulations on different blade profiles. Unfortunately, time and knowledge does not reach far enough here, for what eventually is referred to a potential future work. The NACA0018 blade profile (figure 4.2) is often used in helical turbines and will be assumed as a temporary optimum which is capable for improvement. Also Niblick considered this type as usable for his experiments [2]. In a later design of the actual airfoil, tests for an optimal shape are inevitable in any case and this shape might then be good to start from. Obviously, this hollow profile should be adapted by a solid structure in order to withstand the high water pressure.

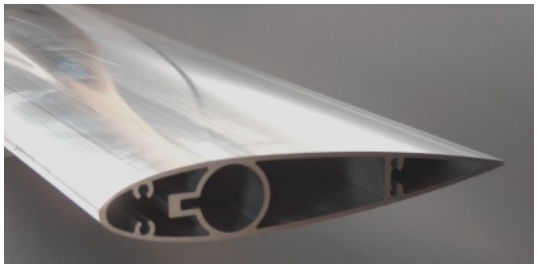

Figure 4.2: NACA0018 blade profile.

4.2.2 Generator

A coreless axial-flux permanent-magnet generator is deemed to be most suitable seeing our low angular velocities. Many already existing generator models match what we require, thus we logically chose an off-the-shelf generator. After examining many works [18, 19, 20, 22], following characteristics were considered to be important during selection of the optimal generator.

- Zero cogging torque must be pursued in order to achieve optimal self-start.
- Power must be adjusted as much as possible to the 30 W that is calculated in chapter 3, but any safety margin is allowed in order to prevent damage during unexpected high water currents. A perfect power match does moreover not exist and a compromise should be considered.

- Datasheets should be compared, and an optimum should be found for which the angular speed and the required torque to induce this speed should be chosen as low as possible, and the appropriate generated voltage the highest as possible. Higher voltages are necessary to overcome the voltage drops of the semiconductors of the electronics.

- The machine pole number should be chosen the highest as possible for compensation of the low angular velocity owing to equation 2.8.

Qiangsheng Magnets Co., LTD is a manufacturer of PM alternators that offers a generator approximating our requirements. This company makes adapted AFPM generators for small wind turbines and hydropower plants having coreless (ironless) stator designs. The AFPMG260-0.2kW/200rpm is deemed to be the most suitable solution for what could be found. An inner-type shaft-spin type and outer-rotor housing-spin type can be separated. Both have exactly the same technical parameters. Here, an outer-rotor design is considered to fit better because it has a flatter-disc shape. The housing-spin also facilitates connecting the electronics, because, in this way, they can easily be mounted besides the generator disc instead of at the extension of the shaft. The turbine's height may thus increase a bit by this choice. Examining the generator datasheet yields in sequential order following technical data [28]

- Figure 4.3 shows how the generator structure is adapted;

- Figure 4.4 shows a picture and attached sectional drawings;

- Table 4.1 enumerates subsequently technical parameters concerning electrical and mechanical parameters;

- Table 4.2 represents the company's testing data;

- Figures 4.5, 4.6 and 4.7 represent curves of speed to power, speed to voltage, and speed to torque, respectively.

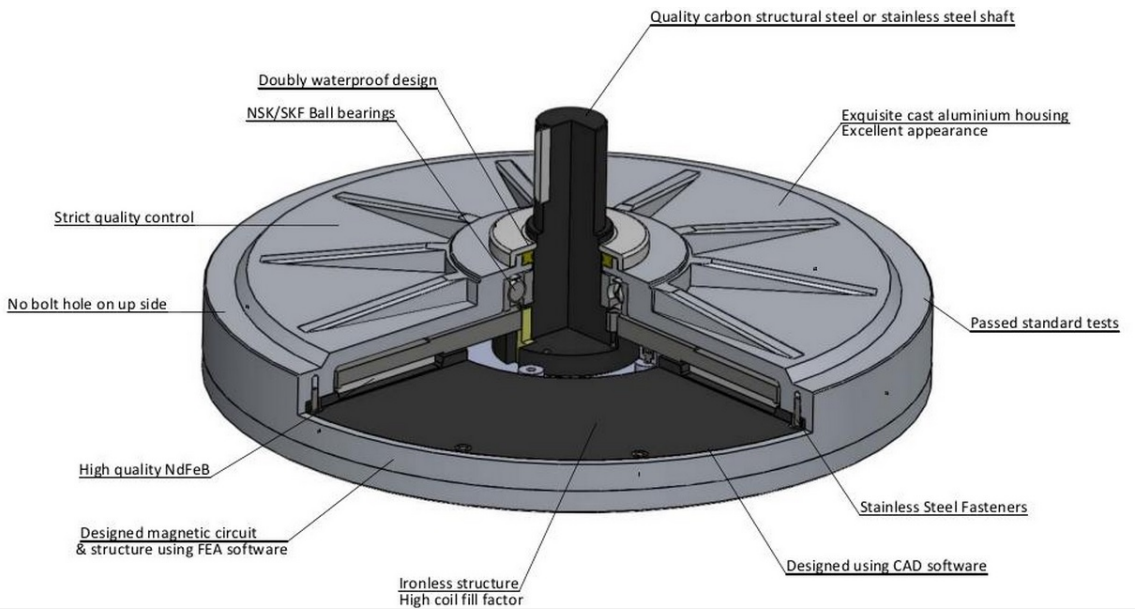

Figure 4.3: Structure of Qiangsheng Magnets Co. LTD AFPMG [28].

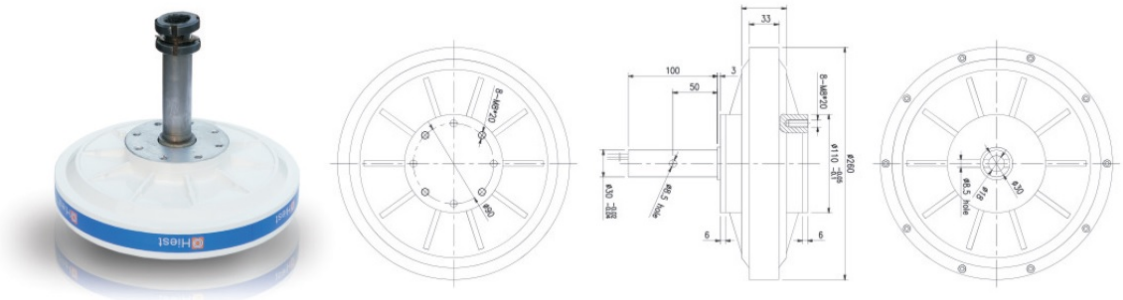

Figure 4.4: AFPMG-0.2kW/200rpm [28].

No.	Parameter	Units	Data
1	Rated output power	KW	0.2
2	Rated speed	RPM	200
3	Rated output voltage	VDC	28
4	Rated current	A	7.1
5	Phase resistance	Ω	2.69
6	Output wire square section	mm^2	2
7	Efficiency		>85%
8	Winding type		Y
9	Insulation resistance		100Mohm Min(500V DC)
10	Voltage withstand	ma	<5 ma
11	Insulation		H class
12	Start torque	Nm	<0.1
13	Temperature rise	℃	<80
14	Max. working temperature	℃	<120
15	Generator diameter	mm	260
16	Shaft diameter	mm	30
17	Housing material		Aluminum Alloy
18	Shaft material		Steel or stainless steel
19	Bearing		NSK or SKF
20	Weight	Kg	11
21	Design lifetime	Year	>20

Table 4.1: Technical parameters of AFPMG260-0.2kW/200rpm [28].

Speed (RPM)	Load voltage (VDC)	Load current (A)	Load power (W)	Torque (N.m)	Efficiency （%）
200	28.1	7.1	200	10.6	90.1
180	25.2	6.4	162	9.6	89.5
160	22.5	5.8	130	8.7	89.2
140	19.6	5.3	103	7.9	88.8
120	16.7	4.6	77	7.0	87.9
100	14.1	3.9	55	6.1	86.1
80	11.2	3.2	36	5.0	85.8
60	8.5	2.4	21	3.9	85.1
40	5.7	1.7	10	2.8	84.3
20	2.8	0.9	3	1.5	82.3

Table 4.2: Testing data of AFPMG260-0.2kW/200rpm [28].

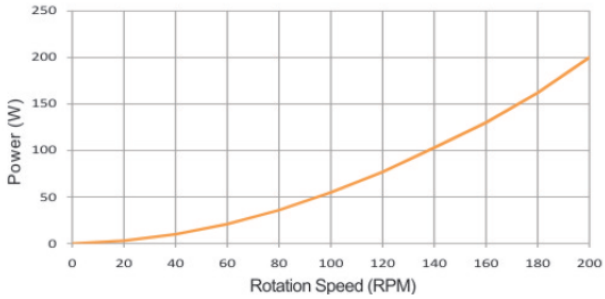

Figure 4.5: Speed-power curve of of AFPMG-0.2kW/200rpm [28].

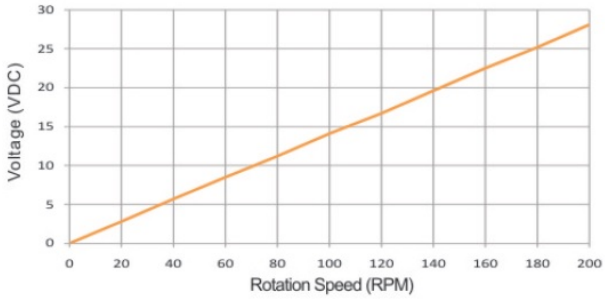

Figure 4.6: Speed-voltage curve of AFPMG-0.2kW/200rpm [28].

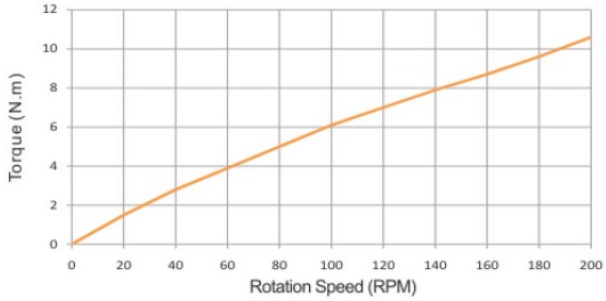

Figure 4.7: Speed-torque curve of AFPMG-0.2kW/200rpm [28].

This generator consists of 10 pole pairs. A higher pole pair should compensate the emerging voltage reduction caused by the lower angular velocity as results in table 4.2 prove. Table 4.1 indicates an obtainable voltage of 28.1 V for an angular velocity of 200 rpm and a torque of 10.6 Nm. Knowing that we aim to have an output voltage of 58.4 V, the generator voltage should still be upconverted as was already expected to be inevitable previously. Hence, a low-power electronic boost converter circuitry should still compensate this too-low voltage. In normal operation, a speed of 200 rpm is expected not to be achieved if the slow water velocity and the maximum capacity of the turbine is encountered. A gear box is superfluous as this is avoided on purpose by reasons of better results.

Observing these data of tables 4.1 and 4.2, and figures 4.5, 4.6 and 4.7 yields some remarks. First of all, the fact that this type is oversized, does not affect the achieved efficiency results too much. According to the manufacturer's testing data, all efficiencies range between 82.3 and 90.1%. Thus, except for the slightly bigger size and weight, this factor does not affect results too much. On the other hand, angular speeds are still supposed to be the highest possible. As figure 4.5 demonstrates power still improves more than directly proportional for an increasing angular speed. Clearly, a higher rotational speed also improves the efficiency of the generator (and moreover because of the corresponding higher voltage, the efficiency of the electronics improves as well). Higher speed also requires higher torque and both parameters are approximately rectilinearly correlated to each other.

4.2.3 Low-Power Electronics

Based on S. Beeby and N. White's scheme represented in figure 2.48 [25], and on several other studies [23, 24], an overall scheme can be composed that might be a good solution for the low-power electronics (figure 4.8). Important characteristics that are required to prove the optimal structure of this schematic are the following:

- A closed-loop design is required for the ability of sending feedback signals to a central control element which is the microcontroller. Hence, this loop can control actively output to the input, and when a deviation compared to the calculated value occurs, this value might be updated by making use of the feedback signals.
- The input voltage is a wild three-phase AC signal ranging between 0 and 28 V, and the output should be a fixed DC voltage of 58.4 V for the battery charger. Since forward voltage drops should be included it is obviously impossible to find components operating close to 0 V .

- Electronics should be selected in the range of the calculated power of chapter 3, 1 to 30 W. Since components are mostly strictly limited in their operating range, it is important to set this parameter correct. Furthermore, efficiencies might strongly decrease for power (or voltage) that deviates too much from the nominal values.

Following elements are implemented in this control loop in order to rectify the voltage, supply an optimal power flow, and adjust the voltage to a fixed, and upconverted output voltage (figure 4.8): rectifier, boost converter, supercapacitor, boost converter and microcontroller (with additional current sense amplifier to measure current). Since results are here highly dependent on the obtained power of the turbine and the generator, and most of the components are moreover found commercially, we will only propose where elements that match our requirements could be found.

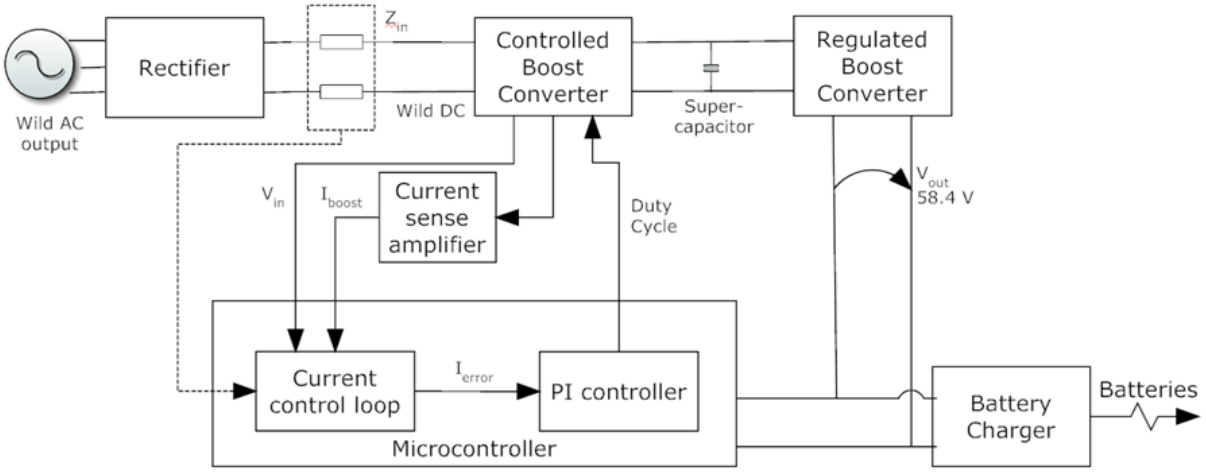

Figure 4.8: Overview of closed-loop low-power electronic scheme.

Rectifier

A three-phase rectifier is connected to the wild AC output of the generator. For an optimal rectifier circuitry, active components are inevitable. Thus, MOSFETS are chosen in order to restrict power losses caused by forward voltage drops and because of the fast recovery time. These executions are commercially available on [29], for which a rectifier should be chosen that withstands the prescribed input range.

Controlled boost converter

A boost converter is controlled by a microcontroller such its input is adjusted to its output impedance as formula 2.19 describes. Correspondingly, its output voltage alternates as well. The microcontroller alters the duty cycle of actively chosen semiconductors for which MOSFETS are again most preferable, by making use of PWM signals. In this boost converter circuitry the MOSFETS operate as gates to chop current signals and corresponding voltage signals in a pulsed signal in order to set the output voltage to a fixed level and the power flow at its maximum.

A three-phase rectifier and impedance matching boost converter can additionally be executed as one circuit which results in a circuit shown on figure 4.9. This circuit can eventually be adjusted in order to reduce components as J.-C Crebier et al. described [30]. Executions of this simplification are commercial available [31, 32].

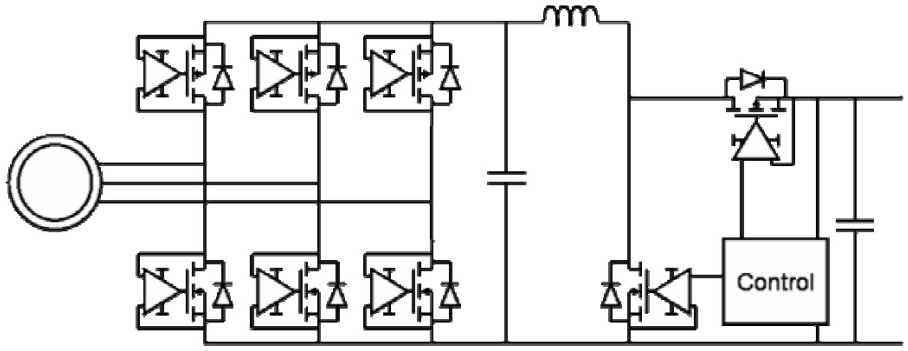

Figure 4.9: A combined circuit of a three-phase rectifier and a boost converter [30].

Supercapacitor

A supercapacitor is connected to the output of the controlled boost converter to flatten the signal in order to reduce voltage oscillations and to reduce the ripple factor as described in equation 2.18. This capacitor should be chosen having the highest capacity as possible and the lowest impedance in order to achieve a more flatten ripple. Furthermore, the operation voltage of this capacitor should be set at the expected output of the matching boost converter.

Boost Converter

A boost converter subsequently upconverts the previously stabilized voltage to a fixed output of 58.4 V. Its input should be chosen again at the same level as the output of the impedance-matching boost converter and the supercapacitor. Many commercially solutions are here available as well [29].

Microcontroller

The electronic loop is closed by a microcontroller. This element operates here as a control unit for the impedance match and fulfils several roles as described in chapter 2. For executing the measuring section, the operating voltage of this microcontroller should be adjusted to the prescribed supplied voltage range of the generator. A current sense amplifier is utilized to transform the measured current to a proportional voltage which is required for processing in the microcontroller. This is performed by measuring the voltage over a linear resistor that is proportional to the necessary current. Further, a control scheme should be configured in the microcontroller which calculates the optimal duty cycle for every current level in order to guarantee a fixed voltage at the output of the boost converter which might result, eventually, in an optimal power flow (figure 2.47).

4.3 Configuration

To implement our proposed energy system a structure is proposed where the turbine is installed in the metal framework as may be observed (figure 3.1 and 4.10). The height of the prototype is about 1.40 m, and the width and length about 1.50 m. Since the turbine and generator have to be connected to one shaft and all of this has to fit under the prototype's framework, the height of the turbine is restricted to 0.80 m and the diameter to 0.50 m. The thickness of the generator is about 0.10 m and the diameter is 0.26 m. Additionally, a box having a height and length of 0.20 m and a width of 0.40 m is considered for enclosing the generator and the attached electronics by which the electronics are placed besides the generator disc. The protection box should be sealed against the high water pressure at the place where the shaft enters the box, but this is beyond the scope of this work.

The motivation for our well-considered structure is the following:

- Unused space in the framework is filled in this way, for what the global design remains more or less compact which is in benefit of the vehicle during displacement. Counteracting forces of the turbine can be reduced in this way because of the more symmetric design.

- A vertical-axis emplacement of the turbine is chosen for two reasons. First of all this excludes directionality a lot more than the horizontal-axis equivalent emplacement. Secondary, a horizontal-axis emplacement might cause an unwanted force of the flowing water, by which the vehicle might be lifted and lose its fixed position.

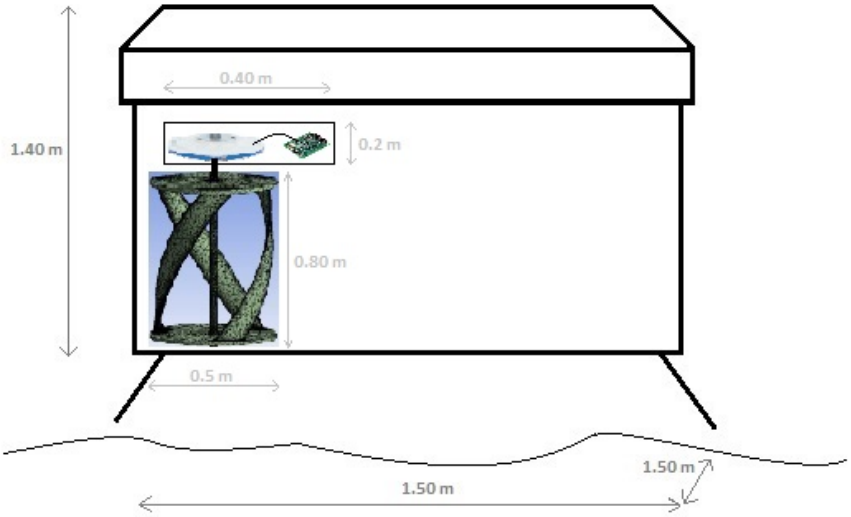

Figure 4.10: Proposal for configuration of energy system.

- This design can be executed such that this structure is easily to take off from the framework if this would be required for any reason.

A possible later improvement might be a shield that surrounds the turbine in order to increase the amount of incoming water, and resulting in a higher angular speed of the turbine. This is a mechanical addition which might be considered after attentive experiments and when the previously described design of the turbine is optimized.

Furthermore the general CPU of the system should be able to disconnect unnecessary loads during start-up. Break-away torque will consequently decrease, resulting in a more fluent start-up at lower speeds.

Chapter 5

Conclusion and Future Work

In this work the most important requirements are set up for autonomous underwater vehicles. After performing an exhaustive analysis, comparing several solutions, a possible structure is proposed for a micro-scale energy harvesting system for powers up to a maximum of 30 W. The following structure is deemed to have optimal results and is considered to be configurable in the vehicle's surrounding framework: a combination of a three-bladed vertical-axis helical turbine, an axial-flux permanent-magnet coreless-stator generator, and a closed-loop power electronic scheme fulfilling rectification, impedance match, voltage stabilization and voltage conversion.

Since this work was meant to finish in a time interval of only three months, unfortunately only a theoretical analyses could be performed. Our developed structure could therefore not be implemented yet, which should be a part of a future work. This study contains the outline for many tests and simulations to create an actual energy harvesting unit. The following steps are proposed to accomplish:

- A turbine might be developed for which our outlined design parameters, together with many other optimal airfoil tests, may lead to an actual execution.
- A coreless axial-flux permanent-magnet generator should be bought for which a configurable model is proposed.
- All low-power electronic components should be purchased and configured as outlined in the proposed closed-loop scheme of this report.
- The complete structure should be tested to draft the energy system's overall characteristics of among others power, voltage, efficiency and starting torque.
- When everything is tested and optimized as much as the system allows, everything should be mounted on the vehicle's framework and tests can be performed in real-ocean conditions.

Bibliography

[1] A. Khaligh and O.C. Onar "Tidal Energy Harvesting" in *Energy Harvesting - Solar, Wind and Ocean Energy Conversion Systems*, Boca Raton, Florida, CRC , 2010, ch 3, pp. 188-192.

[2] A.L. Niblick, "Experimental and Analytical Study of Helical Cross-Flow Turbines for a Tidal Micropower Generation System", M.S. thesis, Dept. Mech Eng., Univ. of Washington, Washington, 2012.

[3] Pump Fundamentals, [Online]. Available: www.pumpfundamentals.com

[4] Coherent Application threads, [Online]. Available: people.bu.edu/dew11/liftanddrag.html

[5] Helix Wind, [Online]. Available: www.helixwind.com

[6] Ampair Energy Ltd, [Online]. Available: www.ampair.com

[7] M. Borghi, "Design, Fabrication and Installation of a Hydrodynamic Rotor for a Small-Scale Experimental Ocean Current Turbine", *SoutheastCon*, Orlando, FL, 2012, pp. 1-6.

[8] F. Scherillo et al., "Numerical and Experimental Analysis of a Shrouded Hydroturbine", *ICCEP*, Ischia, 2011, pp. 216-222.

[9] Solar Excluss, [Online]. Available: www.solar.excluss.com

[10] T. Maître, E. Amet, C. Pellone, "Modeling of the flow in a Darrieus water turbine: Wall grid refinement analysis and comparison with experiments", Grenoble, 2012, doi:10.1016/j.renene.2012.09.030

[11] T. Ikoma et al. "Characteristics of Hydrodynamic Forces and Torque on Darrieus Type Water Turbines for Current Power Generation Systems with CFD Computations", *OCEANS*, Kobe, 2008, pp. 1-8.

[12] tjskl.org.cn, [Online]. Available: www.tjskl.org.cn/

[13] Avstop, [Online]. Available: www.avstop.com/ac/flighttrainghandbook/angleofattackandlift.html

[14] Windpower Engineering, [Online]. Available: www.windpowerengineering.com/

[15] Smart Blade, [Online]. Available: www.smart-blade.com

[16] A. Ludovic, "Vortex Generators", [Online]. Available: Smartcockpit.com

[17] Aerospaceweb, [Online]. Available: http://www.aerospaceweb.org/

[18] M. Hongzhong, "Feasibility Research on DC Generator Based Wind Power Generation System", *SUPERGEN*, Nanjing, 2009, pp. 1-5.

[19] H. Qingling and W. Qunjing, "Design techniques for reducing cogging torque in low-speed permanent magnet wind power generator", *ICEMS*, Beijing, China, 2011.

[20] J. Gieras, R. Wang and M.Kamper, *Axial Flux Permanent Magnet Brushless Machines*, 2nd ed. Netherlands: Springer, 2008.

[21] G. Madescou et al, "Low Speed PM Generator for Direct-Drive Wind Applications", *EUROCON*, Lisbon, Portugal, 2011, pp. 1-4.

[22] W. Jara, A. Martin, J.A. Tapia, "Axial flux PM machine for low wind power generation", *ICEM*, Rome, 2010, pp. 1-5.

[23] M.H. Rashid, *Power Electronics Handbook*, 2nd ed., Pensacola, FL: Academic Press, 2010.

[24] J.W. Kolar, "The Essence of Three-Phase PFC Rectifier Systems", *Telecommunications Energy Conference*, Amsterdam, 2011, pp. 1-27.

[25] S. Beeby and N. White "Power Management Electronics" *Energy Harvesting for Autonomous Systems*, Norwood: Springer, 2010, ch 6.

[26] Thefutureofthings.com, [Online]. Available: www.thefutureofthings.com

[27] H. Ferreira et al., "TURTLE – Systems and technologies for Deep Ocean long term presence", *OCEANS*, St. John's, NL, 2014, pp. 1-10.

[28] Qiangsheng Magnets Co., LTD, [Online]. Available: www.qm-magnet.com

[29] www.ti.com

[30] J.-C Crebier et al. "High Efficiency 3-Phase CMS Rectifier with step up and regulated", *DTIP*, Stresa, 2007, pp. 338-343.

[31] www.maxim-ic.com

[32] www.linear.com

[33] Vortex Hydro Energy, [Online]. Available: www.vortexhydroenergy.com

[34] S.P. Adhau, "A Comparative Study of Micro Hydro Power Schemes Promoting Self Sustained Rural Areas", *SUPERGEN*, Nanjing, 2009, pp. 1-6.